

Anonymous Referee #1

This paper is the overview paper for a special issue on the SAFIRED experiment, and is intended to introduce the project, provide details on the instrumentation, meteorology, and give a brief synopsis of the results that will be discussed in the individual papers. This paper does a reasonable job of this, although with a number of places that require some clarification (see below). One major drawback with this paper is that it is too long and spends too much time and detail on the results. Presumably, those results are covered in detail in the individual papers.

Another problem is that the text in almost all the figures is too small to read, and the time needs to be defined, is it local time?

The authors thank the referee for their comments and suggestions. The manuscript has undergone numerous changes, including removing or shortening sections that were previously too long. Furthermore, figures now have a higher resolution and with larger text. The date and time has also been defined as local time within the figures and discussion.

Abstract; This section is too long and needs to be tightened up considerably. There are also the following problems:

Line 45. How does one measure the “mercury cycle”? It is possible to measure the chemical species that make up the mercury cycle.

Line 47. The word “emitted” is redundant.

Lines 52 and 53. What distinguishes ‘intense’ and ‘close’ smoke plumes?

Lines 59 and 60. These few sentences are examples of extraneous material not appropriate to an abstract.

(now L47) The term "mercury cycle" has been replaced with "speciated atmospheric mercury".

(now L49) The word "emitted" has been removed.

The sentence discussing "intense or close" smoke plumes has been removed.

(now L61) The last section of the abstract has been replaced with a concise sentence summarising the content of the manuscript.

Introduction:

Lines 80 and 81. Savannah and grassland fires are not the largest source of carbon to the atmosphere, as is clear when comparing the numbers from the quoted references with the global anthropogenic source of CO₂ for example. Do the authors mean the largest source of black carbon?

*(now L91) This sentence has been amended to mention that savannah and grassland fires are the largest source of carbon emissions **from biomass burning**.*

Line 109. NO_x is not an incomplete combustion product, in fact NO is most definitely a flaming stage compound. The authors would know this if they referred to the numerous references that have come after Crutzen and Andreae [1990], Akagi et al [2011] (referenced later on) is a nice recent review of BB emissions.

(now L119) "Incomplete combustion" has been changed to "combustion processes".

Description of experiment;

Line 194. If this is meant to be only place the details of PTRMS calibration is discussed, then we need a reference or further explanation for calculating approximate response factors.

The discussion of instrument calibrations has been removed from the manuscript.

Line 241. The term PBM need to be defined here.

(now L294) Particulate-bound mercury (PBM) has now been defined at the first point of mention.

Lines 256-258. Doesn't the CO₂ from fires mess with the 'transfer velocity' measurements?

(now L312) The transfer velocity and CO₂ measurements were taken with two different instruments, as indicated.

Lines 265-267. The half-life of Radon is much longer than that of NO_x (which is about 3-4 hours) about the same as SO₂, and shorter than aerosols (which is about 2 weeks), not sure how to think about water vapor.

(now R316) The section discussing Radon has been significantly shortened and this sentence is no longer present.

Line 307. What is a 'Total Suspended Particulate style inlet'? I've never heard of this, so it needs to be explained further or a reference given that explains it.

(now L374) The TPS inlet has now been given a brief description

Line 335. Are you saying that the extracts have not been analyzed yet?

(now L409) "These extracts will be analysed..." has been changed to "These extracts have been analysed".

Overview of the Campaign;

Lines 446-450. Isn't it both boundary layer mixing and time spent over land that determine Rn concentrations? This section needs a better explanation of how these two effects were differentiated.

(now L547) This section has been altered in the context of the biomass burning periods (BBPs). Both the diurnal variations and the variations in the magnitude of radon concentrations across different BBPs at the same daily hour provide insight into the boundary layer and the terrestrial residence time.

Line 457 and Table 1. The term “background concentration” is difficult to define and is not consistently applied in this paper. Those medians should not be considered “background” values. Background to me means the value that would be observed in the absence of a continental source (urban, fire etc.). This is particularly true for CO, 130ppbv is much higher than background, which is probably around 90. I point out that later in the paper, (line 554) much lower numbers were quoted for O3 and CO, 10 ppbv and 66ppbv, which are obviously too low. Table 1. The measurements do not justify the number of significant figures reported for most of these quantities.

The table with the summary measurements has been removed along with the discussion of "background concentrations".

Figure 5 Caption. Plot (d) is mistakenly attributed to ‘nitrogen dioxide’ and should be nitrous oxide.

(now Figure 3) This has been fixed.

Figure 6. The legends and scale insets are too small and, in one case, not next to the panel to which they refer.

(now Figure 4) This has been fixed.

Lines 496-498. It is well known in the community that the AMS technique does not work for much of the chloride that one finds in the atmosphere, particularly near coasts, because it is in the form of refractory salts. What is worse is that because of background subtraction issues, other chloride is actually under-measured. Fires likely emit chloride as ammonium chloride, which is volatile and will be measured by AMS. These are probably the main reasons for your observations.

Lines 504-506. Another cause of this effect is the above limitation of the AMS instrument.

(now L813) The speculation of the origin of chloride being due to the coastal location has been removed.

Lines 553-558. The ratio $\frac{O_3}{CO}$ is not a good indicator of photochemical age or processing. One only has to look at the high O3 plume during BBP4 (6/26 as far as I can tell), which reaches 100ppbv. This obviously had substantial photochemical processing, how else does that much O3 get made? Yet the ratio is low, probably because the CO had not been mixed out as much as in the other plumes. You need to find some other indicator.

(now Figure 7) $\frac{O_3}{CO}$ data and the discussion of it has been removed from the manuscript. Acetonitrile and toluene data has been included and their ratios have been discussed in the context of photochemical processing.

Line 623. The authors seem to be ignoring the high O₃ plume during BBP4 which indicates faster O₃ production in this plume. This would seem to be one of the more interesting observations of this study.

(now Figure 4) The spike in the O₃ during BBP4 has been attributed to cross-contamination within the ozone analyser. Substantial photochemical processing of that plume was highly unlikely given large concentrations observed more than 4 hours after sunset, observed fire proximities, and indicators within the AMS (e.g f44).

Anonymous Referee #2

Received and published: 23 December 2016

Mallet et al. provide an overview of the multi-institutional measurement campaign conducted in Northern Australia during the dry season to measure the emissions and transformations of trace gases and particles emitted by savannah and grassland fires. The motivation for the measurement campaign is novel, the manuscript is well written and the results are appropriately described. The measurements from this campaign are likely to improve our understanding of biomass burning emissions at the local and global scale. The only major concern I have is that the manuscript, being an overview article, could be improved in terms of the presentation of the campaign specific information and data (see comment #s 3, 4, 5, 11, 12). This would make the manuscript much more citable and a serve as a gateway for anyone interested in SAFIRED-related literature. I recommend publication of the manuscript after the following minor comments have been addressed and/or clarified.

The authors thank the referee for their comments and suggestions. We have taken these on board and have improved the quality of the manuscript accordingly.

The resolution of the figures is too poor and needs to be fixed. I would ask the authors to consider using vector images.

The font size on the figures in some cases is too small and very hard to discern on a printed copy of the manuscript.

The resolution of the figures has been improved (either larger files or .eps format) and the font size has been increased.

While some of the relevant literature has been cited, it would be worthwhile to discuss (likely in the Introduction) similar measurement campaigns performed in other parts of the world that have examined emissions from biomass burning and how those earlier lab and field efforts (e.g., BBOP, SCREAM, FLAME1-5, etc) have helped inform critical gaps, research questions, instrumentation, analysis techniques etc. for the SAFIRED campaign.

(L151) A short discussion of previous field and laboratory measurements has been added to the end of the Introduction.

Being an overview article, I think the manuscript could benefit from a schematic and/or cartoon in the introduction that sketches the region of interest (Northern Australia) and caricatures the emissions, processes and impacts being studied in detail in this campaign. Furthermore, a bulleted list in the beginning of the manuscript that lists the research/science questions for SAFIRED would provide context for the various measurements and analysis performed.

(L 164) The authors think that a schematic/cartoon is not appropriate for this publication. A bulleted list at the end of the Introduction has been added, however.

In the methods section, the manuscript could benefit from a Table that lists the instrument, quantity measured, accuracy/precision, frequency. For example, see Figure 1b, 1c, 2b, 2c, etc in Ryerson et al., (JGR, 2013).

(L196 and Table 1) A table summarising the quantities measured and the instruments used has been included at the beginning of the Instruments and measurements section.

In some cases (e.g., non methane organic compounds), too much detail is provided in the methods section describing the measurement.

The discussion of calibration techniques used in the NMOC measurements has been removed for concision and consistency with the other measurements.

I did not bother to investigate this further but I wasn't quite sure what the technical definition of the word 'fetch' is. It might be helpful to clarify this for the reader.

This term is no longer present within the manuscript.

Too many significant figures (up to 6!) for some of the measurements in Table 1.

This table was superfluous and has been removed from the results section.

Figure 7: Are those raw SMPS data or lognormal fits to the SMPS data? The distributions look uncannily smooth.

(now Figure 8) The data presented in this figure are averaged raw SMPS data. They are smooth due to unimodal shape and little variation in the size distributions during each BBP.

Line 590: The word ‘aging’ is commonly used to refer to chemical reactions but in the example is used here to refer to thermodynamics.

(now L820) The evaporation of organic compounds typically occurs after some sort of chemical reaction, but there is no reason that the evaporation of organic compounds cannot be included within "aging processes".

The ‘Outcomes’ section could benefit from the following: (i) discussion of the results in the context of earlier work and how the findings here are similar or different,

(ii) how the SAFIRED measurements were insightful (iii) what questions still remain unanswered, and (iv) directions for future work.

Similar to comment 5, a Table listing the companion publications and its central finding would be helpful for the interested reader to track the measurement-specific paper.

The "Outcomes" section has been significantly altered. A summary table listing the companion publications has been included at the beginning of this section. A lot of "background"-like text has been removed so that more of a focus has been placed on the all of the outcomes and future work.

Line 658-677: Will the NMOC emissions and speciation be discussed in a forthcoming publication? I did not see a SAFIRED-related reference for this section.

(L1002) A manuscript containing the NMOC data and discussion has not been finalised at the time of this response and submission of this version of the manuscript. However, this data is currently being examined and will be published in the future. This has been indicated.

Line 762-763: How does primary organic aerosol interact with NMOCs to form SOA? I am not sure this sentence is phrased correctly. Do you mean primary organic aerosol serves as a seed for the SOA produced from NMOC oxidation?

This sentence and section has been removed from the manuscript. The referee was correct in their interpretation.

Clarification question: Were aircrafts used to study the biomass burning plumes?

While I understand that the majority of the companion papers that deal with the specifics of each measurement are in the process of being prepared or are currently under review, are there any novel campaign-wide conclusions that the authors would like to discuss in the concluding section of the manuscript?

(L1217) The "Looking forward" section has been changed to "Conclusions and looking forward". A paragraph summarising the campaign-wide conclusions have been included at the beginning of this section. Aircrafts were not used in this study. Several recommendations have been amended to the end of this section, including taking in situ measurements at the surface and throughout the boundary layer.

Anonymous Referee #3

Received and published: 8 December 2016

This paper gives an overview of the SAFIRED2014 campaign in Northern Australia aimed at investigating biomass burning in an area that has very frequent burning but is clearly understudied. This paper suffers from the typical issues of overview papers, where there is a long introduction of instruments and methods, but no actual results. In this paper especially the last section “Outcomes of SAFIRED” is very long, includes short literature reviews, but teases at potential results and points to other related papers without giving any results. Overview papers clearly serve a purpose and should include four major points: 1) description of the science goals and how the campaign was designed to answer them, 2) a systematic description of the used instrumentation, 3) a big picture overview of the results and 4) a conclusion of how the campaign results are usable for answering the science question. This overview paper here describes most of the above points, but could benefit from some improvements and in particular would benefit from summarizing the results more systematically.

The authors thank the referee for their comments and suggestions. The manuscript has been significantly altered in order to avoid the problems that the referee finds common in overview papers. More emphasis has been placed on the results and introductory text has been removed or shortened, especially within the "Outcomes of SAFIRED" section.

Specific Comments:

I think it would be helpful to actually list the specific science questions at the end of the introduction or in a new section before the instrument descriptions.

(L164) The specific science questions have been summarised at the end of the Introduction section.

Instruments and Measurements

The chapter 2.2 Instruments and Measurements should be made more consistent between the individual instrument descriptions and also misses some critical information. Most of the instrument detection methods are described well, but the most important information for all the measurements are missing. For each instrument description the following needs to be added: sensitivity (precision and accuracy), limit of detection, time resolution and used inlet. A table should be added that lists all of these instrument parameters and also a reference to the technique. The Radon instrument description also includes a summary of how Radon measurements are used in atmospheric research. This is not appropriate here and should be moved to the results section around page 21.

(L196 and Table 1) A table has been added to this section, giving a summary of the Instruments and Measurements (quantity, instrument, time resolution, reference;

other details are discussed in relevant companion or referenced studies). The summary of the use of Radon measurements in atmospheric research has been mostly removed or moved to later sections.

The chapter Aerosols should be numbered consistently with 2.2.2 Fires and Air Masses

(L360) This has been fixed.

What I was mostly missing in this chapter was putting SAFIRED into the bigger picture of fire emissions in Australia, e.g.: how representative is SAFIRED, was this a typical year and what could SAFIRED potentially tell us about emission estimates in northern Australia. How many fires did you observe during SAFIRED? How many of those measured plumes were fresh (for emission ratios) and how many were aged?

With a more concise manuscript, the focus is now on the bigger picture of fire emissions in Australia. Without long term in situ measurements it is difficult to conclude whether the 2014 early dry season was atypical or not. This has been discussed in the "Conclusions and Looking Forward" section.

Given the high frequency of fires across the regions and the mixing and differing trajectories of smoke plumes, it is difficult to attribute the constantly elevated signals to individual (fresh or aged) plumes. Nonetheless, a lot of the discussed of the spikes in the gaseous and aerosol species in the "Result" section is devoted to trying to link the measured emissions to fires. Furthermore, the two companion papers, Desservattaz et al., 2017 and Milic et al., 2016, provide in-depth investigations of the identification of individual plumes, emission factors and the atmospheric aging processes of aerosol during SAFIRED.

Figure 4: The data here are split into weak moderate and strong mixing, but nothing is really done with this separation later. Also the differences are not very strong. In the next Figure and the rest of the manuscript the data get separated into different BB and coastal periods. This seems a better separation. I suggest removing the mixing categories. I am also wondering how the wind direction plot looks for the Coastal Period. This would be more helpful for a separation.

(now Figures 5 and 7) The data has been split into the BBPs and CP rather than "mixing" category. Diurnal trends of radon, wind speed, wind direction, temperature and select VOCs for each period have been displayed. The same has been done for the greenhouse gases and aerosol species and size and is displayed in the supplementary material.

Figure 4c y-axis should go from 0-360.

(now Figures 5 and 6) Because the wind direction never was between 200° and 360°, the axis has been kept from 0° to 200° so that variations are more easily distinguished.

page 24 line 473: What are the criteria used to separate the data into these periods? The separation seems very arbitrary to me, especially what is the difference between BBP2 and BBP3. Also the coastal period has large CO mixing ratios and very similar O3/CO ratios as BBP3. Please explain in more detail what is difference between the periods and how you define BBP. Are these by CO or acetonitrile enhancements, back trajectories, or fire counts? diurnal trend e.g.:

(now L489) There was no strict criteria in separating the data into the 5 different periods. A combination of the daily satellite observed fires and the meteorological, gaseous and aerosol measurements were used to distinguish periods with BB and marine influence. Furthermore, the BB periods were selected as full days and the CP was selected as 1.5 days exactly to provide further insight into the diurnal variations

page24 line 470-471: The authors argue here and in other places that the diurnal variations are caused by the mixing height. This is probably right, but no actual evidence is presented. The wind direction changes as can be seen clearly in Figure 4. Looking only at the time series in Figures 5 and 6 one cannot judge, if the diurnal changes align with wind direction change or more with the Radon profile. A diurnal profile of some trace gases and aerosol species should be added. I would also like to see that separated for the different BBP and CP.

(now L546) It now reads that mixing height, wind velocity, fire locations and the time of fires are the cause of the diurnal variations. Diurnal variations have been separated into the BBPs and CP.

Figures 5 and 8. It would be good to also show the CO data on a linear scale.

(now Figures 3 and 7) The CO data has now been presented on a linear scale.

Close Proximity Fires versus Aged Fires

On several places on pages 27-30 the age of fire plumes are discussed in rather vague terms sometimes using organic aerosol or size distributions as chemical indicator in addition to the fire locations. To show photochemical aging the most commonly used way is to look at ratios of a short lived tracer to an inert tracer on the time scale of the transport. Ratios of some of the VOC measurements versus CO or acetonitrile would be best used to show aging, most commonly used are aromatic species, benzene for longer time scales, toluene or larger aromatics for shorter time scales. Enhancement ratios of fresh fires seem to be available from the “close proximity fires” or nighttime fire plumes, although I have my doubts about how close those fires were, as I will describe below. Fires in the region are relatively similar and the emission ratios should therefore also be similar enough to distinguish between fresh plumes and plumes transported over 200-300km to the site using VOC/CO ratios. I would suggest replacing all the vague discussions about plume age with adequate VOC/CO enhancement ratios.

O₃/CO ratios: The O₃/CO is used in Figures 5 and 8 and is described as giving an indication of photochemical age. Unfortunately O₃/CO are much more complicated than that and depend on many different factors such as VOC/NO_x ratios such that the ratio really cannot be used as “photochemical age”. I think for this paper here, it is best to remove the O₃/CO ratios instead of adding a proper explanation.

The ozone enhancement shown in Figure 8 for the close proximity fire is substantial and ozone values of almost 100ppb are detected in the plume. This means that there has been significant photochemical processing of potentially several hours during plume transport. If the plume would be really fresh, ozone would actually be titrated. Again VOC/CO could be very helpful here and should be looked into. Also a comparison to a nighttime plume measurement would be very useful. Again, I doubt that this plume is very fresh.

The ozone spike during BBP4 was likely a result of cross contamination within the ozone analyzer from other UV-absorbing species. High concentrations, the time of evening and a low f44 value from the AMS indicate very fresh smoke and this is supported by observations of the burned area. O₃/CO ratios have been removed from the manuscript and all discussion and data has been replaced with acetonitrile, toluene and their ratio (Figure 7).

Outcomes of SAFIRED

The paper is rather long in its current form and in particular this chapter is more of a literature review, of what could potentially be done with the specific measurement. I actually think this is not appropriate for an overview paper and

would be more appropriately discussed in the detailed follow-up papers. I suggest deleting this whole section

and just briefly mentioning the potential major outcomes in the “Looking Forward” section.

The Outcomes of SAFIRED section has been shortened and does no longer include "background" text which, as the referee points out, is not appropriate for this section. This section now gives a brief overview of the campaign papers and the overall results from the study.

The picture quality of all Figures needs to be improved.

The resolution and file format has been improved and font sizes have been increased.

1 **Title: Biomass burning emissions in north Australia during the early dry season:**
2 **an overview of the 2014 SAFIRED campaign**

Formatted: Font color: Text 1

Formatted: Font color: Text 1

3 **Authors:**

4 Marc D. Mallet¹, Maximilien J. Desservettaz², Branka Miljevic^{1*}, Anđelija Milic¹,
5 Zoran D. Ristovski¹, Joel Alroe¹, Luke T. Cravigan¹, E. Rohan Jayaratne¹, Clare Paton-
6 Walsh², David W.T. Griffith², Stephen R. Wilson², Graham Kettlewell², Marcel V. van
7 der Schoot³, Paul Selleck³, Fabienne Reisen³, Sarah J. Lawson³, Jason Ward³, James
8 Harnwell³, Min Cheng³, Rob W. Gillett³, Suzie B. Molloy³, Dean Howard⁴, Peter F.
9 Nelson⁴, Anthony L. Morrison⁴, Grant C. Edwards⁴, Alastair G. Williams⁵, Scott D.
10 Chambers⁵, Sylvester Werczynski⁵, Leah R. Williams⁶, V. Holly L. Winton^{7,n}, Brad
11 Atkinson⁸, Xianyu Wang⁹, Melita D. Keywood^{3*}

Formatted: Normal

12 **Affiliations:**

13 ¹Department of Chemistry, Physics and Mechanical Engineering, Queensland University of Technology,
14 Queensland, Brisbane, 4000, Australia

15 ²Centre for Atmospheric Chemistry, University of Wollongong, Wollongong, New South Wales, 2522,
16 Australia

17 ³CSIRO Oceans and Atmosphere, Aspendale, Victoria, 3195, Australia

18 ⁴Department of Environmental Sciences, Macquarie University, Sydney, New South Wales, 2109,
19 Australia

20 ⁵Australian Nuclear Science and Technology Organisation, Sydney, New South Wales, 2232, Australia

21 ⁶Aerodyne Research, Inc., Billerica, Massachusetts, 01821, USA

22 ⁷Physics and Astronomy, Curtin University, Perth, Western Australia, 6102, Australia

23 ⁸Bureau of Meteorology, Darwin, Northern Territory, 0810, Australia

24 ⁹National Research Centre for Environmental Toxicology, Brisbane, Queensland, 4108, Australia

25 ⁿNow at the British Antarctic Survey, Cambridge, CB3 0ET, United Kingdom

Deleted: National Environmental Research Council,

Deleted: 0HT

Formatted: Font color: Text 1

Deleted: K

Formatted: Font color: Text 1

29 ***Corresponding Authors:**

30 Dr Melita Keywood

31 Contact Phone: +613 9239 4596

32 Contact Email: melita.keywood@csiro.au

33

34 Dr Branka Miljevic

35 Contact Phone: +61 7 3138 3827

36

37 Contact Email: b.miljevic@qut.edu.au

38 **Keywords:**

39 Biomass burning | savannah fires | greenhouse gases | aerosols | mercury

40 **Abstract**

41

42 The SAFIRED (Savannah Fires in the Early Dry Season) campaign took place from
43 29th of May, 2014 until the 30th June, 2014 at the Australian Tropical Atmospheric
44 Research Station (ATARS) in the Northern Territory, Australia. The purpose of this
45 campaign was to investigate emissions from fires in the early dry season in northern
46 Australia. Measurements were made of biomass burning aerosols, volatile organic
47 compounds, polycyclic aromatic carbons, greenhouse gases, radon, ~~speciated~~
48 ~~atmospheric mercury~~, and trace metals. Aspects of the biomass burning aerosol
49 emissions investigated included; emission factors of various ~~species~~, physical and
50 chemical aerosol properties, aerosol aging, micronutrient supply to the ocean,
51 nucleation, and aerosol water uptake. Over the course of the month-long campaign,
52 biomass burning signals were prevalent and emissions from several large single burning
53 events were observed at ATARS.

54 Biomass burning emissions dominated the gas and aerosol concentrations in this
55 region. Dry season fires are extremely frequent and widespread across the northern
56 region of Australia, which suggests that the measured aerosol and gaseous emissions at
57 ATARS are likely representative of signals across the entire region of north Australia.
58 Air mass forward trajectories show that these biomass burning emissions are carried
59 north west over the Timor Sea and could influence the atmosphere over Indonesia and
60 the tropical atmosphere over the Indian Ocean. ~~Here~~ we present characteristics of the
61 biomass burning observed at the sampling site and provide an overview of the more
62 specific outcomes of the SAFIRED campaign.

Deleted: mercury cycle

Formatted: Font color: Text 1

Deleted: emitted

Formatted: Font color: Text 1

Formatted: Justified, Indent: First line: 0.39", Line spacing: double

Deleted: . Nine major biomass burning events were identified and associated with intense or close individual smoke plumes

Formatted: Font color: Text 1

Deleted: .

Formatted: Font color: Text 1

Formatted: Font color: Text 1

Formatted: Font color: Text 1

69 **1. Introduction**

Formatted: Font color: Text 1

70 Tropical north Australia is dominated by savannah ecosystems. This region consists of
71 dense native and exotic grasslands and scattered trees and shrubs. Conditions are hot,
72 humid and wet in the summer months of December through March with hot, dry
73 conditions for the rest of the year giving rise to frequent fires between June and
74 November each year. Human settlements are relatively scarce in northern Australia,
75 outside of the territory capital, Darwin (population of 146 000). To the north of the
76 continent are the tropical waters of the Timor Sea, as well as the highly populated
77 Indonesian archipelago. South of the savannah grasslands are the Tanami, Simpson and
78 Great Sandy Deserts, spanning hundreds of thousands of square kilometers. Emissions
79 from fires in the savannah regions of northern Australia are therefore the most
80 significant regional source of greenhouse and other trace gases, as well as atmospheric
81 aerosol. Globally, savannah and grassland fires are the largest source of carbon
82 emissions [from biomass burning](#)(van der Werf et al., 2010;Shi et al., 2015) and play a
83 significant role in the earth’s radiative budget. It is therefore important to quantify,
84 characterise and fully understand the emissions from savannah fires in northern
85 Australia, taking into account the complexity, variability and diversity of the species
86 emitted.

Formatted: Font color: Text 1

Formatted: Font color: Text 1

87
88 In Australia approximately 550 000 km² of tropical and arid savannahs burn each year
89 (Meyer et al., 2012;Russell-Smith et al., 2007), representing 7% of the continent’s land
90 area. In the tropical north of Australia, the fires during the early dry season in May/June
91 consist of naturally occurring and accidental fires, as well as prescribed burns under
92 strategic fire management practice to reduce the frequency and intensity of more
93 extensive fires in the late dry season in October and November (Andersen et al., 2005).

Formatted: Font color: Text 1

Formatted: Font color: Text 1

Formatted: Font color: Text 1

Formatted: Font color: Text 1

94 These fires in the early dry season burn with a low to moderate intensity and are
95 normally confined to the grass-layer. Events where fires reach the canopy level are rare.
96 These prescribed burns are an important process for the region and are undertaken by
97 local landholders with permits, as well as government supported bodies and volunteers.
98 There has been a recent push to reinstate traditional Aboriginal fire management
99 regimes in this region (Russell-Smith et al., 2013). Other fire management regimes are
100 implemented in similar environments around the world, such as the savannah
101 ecosystems of Africa (Govender et al., 2006) or the chaparral grasses in the United
102 States (Akagi et al., 2012). In general, fire management regimes are considered to
103 benefit regional biodiversity and can lead to the long-term increase in living biomass,
104 resulting in a reduction of greenhouse gas emissions (Russell-Smith et al., 2013).
105 Quantifying the emissions from dry season fires on regional scales is essential for
106 understanding the impact of these fires on the local and global atmosphere.

Formatted: Font color: Text 1

Formatted: Font color: Text 1

Formatted: Font color: Text 1

Formatted: Font color: Text 1

Formatted: Font color: Text 1

Formatted: Font color: Text 1

Formatted: Font color: Text 1

Formatted: Font color: Text 1

107
108 The components and concentrations of emissions from savannah fires are dependent
109 upon the vegetation and burning conditions. While CO₂ is the primary product of
110 biomass burning (BB), combustion processes also result in the emission of many other
111 trace gases such as CO, CH₄, NO_x, N₂O as well as non methane organic compounds
112 (NMOCs) and aerosol particles composed of elemental carbon, organic carbon and
113 some inorganic material (Crutzen and Andreae, 1990). The state of organics in biomass
114 burning aerosols can vary significantly due to the type of plant material burned, the
115 characteristics of the fires themselves as well as through aging processes in the
116 atmosphere.

Deleted: incomplete

Formatted: Font color: Text 1

Deleted: s

Formatted: Font color: Text 1

Formatted: Font color: Text 1

Formatted: Font color: Text 1

120 The effects of these emissions on radiative forcing are complex. The global average
121 radiative forcing due to biomass burning aerosol-radiation interaction is estimated in
122 the 5th International Panel on Climate Change report as 0.0 W m⁻² with an uncertainty
123 range of -0.20 to +0.20 Wm⁻² (Bindoff et al., 2013). It is well known that greenhouse
124 gases have a positive radiative forcing, heating up the atmosphere. Light absorbing
125 carbon in the aerosol phase will also result in a positive radiative forcing (Jacobson,
126 2001) by absorbing shortwave radiation. Conversely, the presence of aerosol organic
127 and inorganic matter can result in a negative radiative forcing by scattering solar
128 radiation (Penner et al., 1998). In addition, biomass burning has been shown to be a
129 significant source of cloud condensation nuclei (CCN), despite typically being
130 composed of weakly hygroscopic substances (Lawson et al., 2015), due to the high
131 number of particles emitted. This can result in a change in cloud droplet concentrations
132 and volume, thereby influencing cloud formation, albedo and lifetime. The contribution
133 of each species to the overall radiative forcing is also likely to change as smoke plumes
134 age (Liousse et al., 1995). Furthermore, not all biomass burning aerosol will interact
135 with radiation in the same way. For example, fresh BB emissions in the tropics has been
136 observed to be more absorbing than those from boreal forest fires(Wong and Li, 2002).
137 The role of biomass burning emissions is not limited to the Earth's radiative budget.
138 Certain species of emissions (e.g., mercury) can be deposited and sequestered in soil
139 (Gustin et al., 2008), vegetation (Rea et al., 2002) or bodies of water (LaRoche and
140 Breitbarth, 2005).

141
142 [Large-scale studies in Africa](#) (Keil and Haywood, 2003), [North America](#) (Yokelson et
143 al., 2009;Singh et al., 2006), [Europe](#) (Saarikoski et al., 2007), [South America](#) (Ferek et
144 al., 1998) [and Asia](#) (Lin et al., 2013;Du et al., 2011) [have provided valuable insight into](#)

Formatted: Normal

145 [the impact of fire emissions on the regional atmosphere and laboratory measurements](#)
146 [have proved to be useful in understanding the emission factors, composition and](#)
147 [atmospheric processing of these emissions](#) (Stockwell et al., 2014). [Despite this, there](#)
148 is [still](#) a need for a better scientific understanding of the influence biomass burning has
149 on atmospheric composition and air quality (Kaiser and Keywood, 2015), [particularly](#)
150 [around Australia](#). Furthermore, the tropics are disproportionately under-sampled and
151 the atmospheric and ocean processes in these regions are of both regional and global
152 consequence. The SAFIRED campaign will contribute towards better understanding
153 biomass burning emissions and the atmospheric composition in tropical Australia.

Deleted: There

Formatted: Font color: Text 1

Formatted: Font color: Text 1

Deleted: .

Formatted: Font color: Text 1

154
155 [On a more specific level, the SAFIRED campaign was undertaken with the following](#)
156 [objectives:](#)

- 157 • [To obtain Australian savannah fire dry season emission factors for greenhouse](#)
158 [gases, polycyclicaromatic hydrocarbons, gaseous elemental mercury, non-](#)
159 [methane organic compounds, Aitken and accumulation mode aerosols and non-](#)
160 [refractory submicron organic, sulfates, ammonia, nitrates and chlorides.](#)
- 161 • [To understand the emission of mercury from north Australian fires and to](#)
162 [quantify the delivery of mercury to the ecosystem.](#)
- 163 • [To characterise the composition and size of aerosols in the region of north](#)
164 [Australia and to understand the influence and extent of biomass burning on the](#)
165 [total aerosol burden.](#)
- 166 • [To assess the ability of biomass burning aerosol to act as cloud condensation](#)
167 [nuclei and to establish a link between aerosol composition, size and CCN.](#)

Formatted: List Paragraph, Bulleted + Level: 1 +
Aligned at: 0.25" + Indent at: 0.5"

Formatted: Font color: Text 1

- [To assess the fractional solubility of aerosol iron and other trace metals in this region in the context of the potential supply of micronutrients required for marine primary production in the ocean.](#)

Formatted: Font color: Text 1

2. Description of experiment

2.1 Site

Formatted: Heading 2

The Australian Tropical Atmospheric Research Station (ATARS; 12°14'56.6"S, 131°02'40.8"E) is located on the Gunn Point peninsula in northern Australia (see Figure 1). ATARS is operated by the Australian Bureau of Meteorology and the CSIRO (Commonwealth Scientific and Industrial Research Organisation). Standard meteorological measurements (wind velocity, atmospheric pressure, precipitation) run permanently at ATARS and two laboratories are in place for the installation of other instruments. The SAFIRED campaign took place from 29th May 2014 until the 30th June 2014, with personnel and instruments from nine institutes utilising these laboratories to make comprehensive gaseous and aerosol measurements during this period of the early dry season.

2.2 Instruments and measurements

Deleted:

Formatted: Heading 2

187

Table 1 A summary of the quantities measured during SAFIRED and the respective instrument or measurement technique.

188

<u>Quantity</u>	<u>Instrument or Technique</u>	<u>Sample frequency</u>	<u>Reference</u>
<u>CO, CO₂, CH₄ and N₂O</u>	Fourier transform infrared spectrometry	3 minute	(Griffith et al., 2012)
<u>O₃</u>	UV Photometric Ozone Analysis	1 minute	
<u>Non methane organic compounds</u>	Proton Transfer-Mass Spectrometry, high performance liquid chromatography of Supelco cartridge samples; gas chromatography of adsorbant tubes	3 minute; 12 hour; 12 hour	(Galbally et al., 2007); (Cheng et al., 2016); (Lawson et al., 2015)
<u>Polycyclic aromatic hydrocarbons (gas and particle phase)</u>	Gas chromatography and high resolution mass spectrometry of filter and foam samples	24 hour	(Wang et al., 2017)
<u>Gaseous elemental mercury; gaseous oxidised mercury; and particulate-bound mercury</u>	Cold vapour atomic fluorescence spectroscopy	5 minute; 2 hour; 2 hour	(Landis et al., 2002); (Steffen et al., 2008)
<u>Radon</u>	700L dual-flow two filter detector	1 hour	(Chambers et al., 2014)
<u>Aerosol mobility size distributions (14 nm to 670 nm); neutral and charged aerosol size distributions (0.8 nm to 42 nm)</u>	Scanning mobility particle sizer, Neutral cluster and air ion spectrometry	5 minute; 4 minute	(Mirme et al., 2007)
<u>Cloud condensation nuclei concentration (at 0.5% supersaturation)</u>	Supersaturated streamwise continuous-flow of aerosols in a wetted column using thermal-gradient followed by Optical Particle Counting of activated CCN	10 second	(Gras et al., 2007)
<u>Elemental and organic carbon; water soluble ions; and anhydrous sugars (PM1 and PM10)</u>	β + attenuation; ion chromatography; high performance anion-exchange chromatography	12 hour	(Chow et al., 2007b); (Iinuma et al., 2009)
<u>Soluble and total fraction of trace metals (PM10)</u>	High-resolution inductively coupled plasma mass spectrometry analysis of extracted leachates and digests.	24 hour	(Winton et al., 2016)
<u>Non-refractory chemical composition (PM1)</u>	Time-of-flight aerosol mass spectrometry	3 minute	(Drewnick et al., 2005)
<u>Aerosol volatility and hygroscopicity (50 nm and 150 nm)</u>	Volatility and hygroscopicity tandem differential mobility analysis	12 minute (full cycle)	(Johnson et al., 2004)

Formatted: Caption, Keep with next

Formatted: Left: 1", Right: 1", Top: 1.25", Bottom: 1.25", Width: 11.69", Height: 8.26", Header distance from edge: 0.49", Footer distance from edge: 0.49"

Formatted Table

Formatted: Font:8 pt

Formatted: Font:8 pt

Formatted: Font:8 pt

Formatted: Font:Not Bold

Formatted: Font:8 pt

Formatted: Centered, Position:Horizontal: Left, Relative to: Column, Vertical: 0", Relative to: Paragraph, Horizontal: 0.13", Wrap Around

Formatted: Font:8 pt

Formatted: Centered, Position:Horizontal: Left, Relative to: Column, Vertical: 0", Relative to: Paragraph, Horizontal: 0.13", Wrap Around

Formatted: Font:8 pt

Formatted ... [1]

Formatted: Font:8 pt

Formatted ... [2]

Formatted: Font:8 pt

Formatted ... [3]

Formatted: Font:8 pt

Formatted: Font:8 pt

Formatted ... [4]

Formatted ... [5]

Formatted: Font:8 pt

189
190
191
192
193
194
195
196
197
198
199
200
201
202
203
204
205
206
207
208
209

2.2.1 Trace Gases

Greenhouse gases

Continuous measurement of CO₂, CO, CH₄ and N₂O were made using a high precision FTIR trace gas and isotope Spectronus analyser, developed by the Centre for Atmospheric Chemistry at the University of Wollongong. The analyser combines a Fourier Transform Infrared (FTIR) Spectrometer (Bruker IRCube), a pressure and temperature controlled multi-pass cell and an electronically cooled mercury cadmium telluride detector. A detailed description of the instrument and concentration retrieval technique are available in Griffith et al. (2012) and Griffith (1996).

Ozone and other trace gases

A Multi Axis Differential Optical Absorption Spectrometer (MAX-DOAS) was installed on the top of one of the laboratories during the campaign. The technique has been shown to provide the vertical profile of nitrogen dioxide, ozone, sulfur dioxide, formaldehyde, glyoxal and aerosol extinction (Sinreich et al., 2005; Honninger et al., 2004). The MAX-DOAS instrument used in this campaign was designed and built at the University of Wollongong. It consists of a vertically rotating prism capturing scattered solar radiation at different angles (1°, 2°, 4°, 8°, 16°, 30° and a reference at 90°) into a fibre optic that carries the radiation to a UV-Visible spectrometer (AvaSpec – ULS3648). Furthermore, a Thermo Scientific model 49i UV Photometric Ozone analyser was used to measure ozone concentrations.

Deleted: (Griffith et al., 2012) .
Formatted: Heading 2
Formatted: Font color: Text 1
Formatted: Font color: Text 1

Formatted: Font color: Text 1
Formatted: Font color: Text 1
Formatted: Font color: Text 1
Formatted: Font color: Text 1

Formatted: Font color: Text 1

Formatted: Font color: Text 1

211 **Non-methane organic compounds**

Deleted:

212 Online NMOC measurements were made using a high sensitivity Proton Transfer

213 Reaction-Mass Spectrometer (PTR-MS; Ionicon Analytik) using H_3O^+ as the primary

Formatted: Font color: Text 1, Subscript

214 ion. The inlet was 10 m in length and drew air at $5 L min^{-1}$ from 2 m above the roof

Formatted: Font color: Text 1

215 (approx 5.5 m above ground level). The PTR-MS ran with inlet and drift tube

216 temperature of 60 °C, 600 V drift tube, and 2.2 mbar drift tube pressure, which equates

217 to an energy field of 135 Td. The PTR-MS sequentially scanned masses 15-190, with

218 1 second dwell time. The PTR-MS operated with the aid of auxiliary equipment which

219 regulates the flow of air in the sample inlet and controls whether the PTR-MS is

220 sampling ambient or zero air or calibration gas (Galbally et al., 2007).

221

222 [Furthermore, AT VOC \(adsorbent tube Volatile Organic Compounds\) samples were](#)

223 [collected by an automatic VOC sequencer which actively draws air through two multi-](#)

224 [adsorbent tubes in series \(Markes Carbograph 1TD / CarboPack X\). The adsorbent](#)

225 [tubes were then analysed by a PerkinElmer TurboMatrix™ 650 ATD \(Automated](#)

226 [Thermal Desorber\) and a Hewlett Packard 6890A gas chromatography \(GC\) equipped](#)

227 [with a Flame Ionization Detector \(FID\) and a Mass Selective Detector \(MSD\) at CSIRO](#)

228 [Oceans and Atmosphere laboratories. Further details of the sampling and analyses are](#)

229 [given in Cheng et al. \(2016\).](#)

230

231 During sampling, carbonyls and dicarbonyls were trapped on S10 Supelco cartridges,

232 containing high-purity silica adsorbent coated with 2,4-dinitrophenylhydrazine

233 (DPNH), where they were converted to the hydrazone derivatives. Samples were

234 refrigerated immediately after sampling until analysis. The derivatives were extracted

235 from the cartridge in 2.5 mL of acetonitrile and analysed by high performance liquid

Deleted: During the campaign the PTR-MS was calibrated once per day for the following compounds using certified gas standards from Apel Riemer Environmental Inc, USA and Air Liquide Specialty Gases, USA: acetaldehyde, acetone, acetonitrile, benzene, methacrolein, methanol, methyl ethyl ketone, toluene, 1,3,5-trimethyl benzene, m-xylene, chlorobenzene, alpha pinene, 1,2-dichlorobenzene, 1,3,4 trichlorobenzene, dimethyl sulphide and isoprene. Calibration data were used to construct sensitivity plots, which were used to calculate approximate response factors for other masses not specifically calibrated.

Formatted: Font color: Text 1

Formatted: Font color: Text 1

Deleted: NP

Formatted: Font color: Text 1

Formatted: Font color: Text 1

249 chromatography with diode array detection. The diode array detection enables the
250 absorption spectra of each peak to be determined. The difference in the spectra
251 highlights which peaks in the chromatograms are mono- or dicarbonyl DNPH
252 derivatives and, along with retention times, allows the identification of the dicarbonyls
253 glyoxal and methylglyoxal. Further details can be found in [Lawson et al. \(2015\)](#).

Formatted: Font color: Text 1

Formatted: Font color: Text 1

254 **PAHs**

255 PAHs were sampled through a high-volume air sampler (Kimoto Electric Co., LTD.)
256 using a sampling rate typically at $\sim 60 \text{ m}^{-3} \text{ h}^{-1}$. The sampling rate was calibrated using
257 an orifice plate prior to the sampling campaign and the sampling volume was calculated
258 based on the calibrated sampling rate and sampling duration. A bypass gas meter
259 installed on the sampler was used to monitor any anomalous fluctuation of the sampling
260 rate during the sampling period. Particle-associated and gaseous PAHs were collected
261 on glass fibre filters (Whatman™, 203×254 mm, grade GF/A in sheets) and subsequent
262 polyurethane foam plugs respectively. The glass fibre filters and polyurethane foam,
263 along with the field blank samples, were extracted separately using an Accelerated
264 Solvent Extractor (Thermo Scientific™ Dionex™ ASE™ 350) after being spiked with
265 a solution containing 7 deuterated PAHs (i.e. $^2\text{D}_{10}$ -phenanthrene, $^2\text{D}_{10}$ -fluoranthene,
266 $^2\text{D}_{12}$ -chrysene, $^2\text{D}_{12}$ -benzo[b]fluoranthene, $^2\text{D}_{12}$ -BaP, $^2\text{D}_{12}$ -indeno[1,2,3-cd]pyrene,
267 $^2\text{D}_{12}$ -benzo[g,h,i]perylene) at different levels as internal standards for quantification
268 purposes. Concentrated extracts were cleaned up by neutral alumina and neutral silica.
269 Eluents were carefully evaporated to near dryness and refilled with 250 pg of $^{13}\text{C}_{12}$ -
270 PCB (polychlorinated biphenyl) 141 (in 25 μL isooctane) employed as the
271 recovery/instrument standard for estimating the recoveries of the spiked internal
272 standards and monitoring the performance of the analytical instrument. Samples were
273 analysed using a Thermo Scientific™ TRACE™ 1310 gas chromatograph coupled to

274 a Thermo Scientific™ double-focusing system™ Magnetic Sector high resolution mass
275 spectrometer. The HRMS was operated in electron impact-multiple ion detection mode
276 and resolution was set to $\geq 10,000$ (10% valley definition). An isotopic dilution method
277 was used to quantify 13 PAH analytes including phenanthrene, anthracene,
278 fluoranthene, pyrene, benzo[a]anthracene, chrysene, benzo[b]fluoranthene,
279 benzo[k]fluoranthene, benzo[e]pyrene, BaP, indeno[1,2,3-cd]pyrene,
280 dibenzo[a,h]anthracene, benzo[g,h,i]perylene.

281 **Mercury**

282 Total gaseous mercury, gaseous elemental mercury + gaseous oxidised mercury (TGM;
283 GEM + GOM), was sampled from a 10 m mast and measured via gold pre-concentration
284 and cold vapour atomic fluorescence spectroscopy using a Tekran 2537X instrument.
285 Simultaneously, GEM, GOM and [Particulate-bound mercury \(PBM\)](#), were individually
286 measured using a Tekran 2537B connected to a combined Tekran 1130/1135 speciation
287 unit sampling at a 5.4 m height. The sampling train of the 1130/1135 collects first GOM
288 (KCl-coated denuder) then PBM (quartz wool pyrolyser) in series from a 10 L min^{-1}
289 sampling flow, allowing GEM only to flow onwards for detection by subsampling by
290 the 2537B. Due to the small atmospheric concentrations of GOM and PBM, pre-
291 concentration occurred over a 1-hour period with subsequent analysis taking an
292 additional hour. Continuous measurements of GEM at 5-minute resolution were made
293 possible for the 2537B unit by rotating pre-concentration/analysis roles of the two
294 internal gold traps. Both 2537 units sampled at 1 L min^{-1} and were calibrated every 23
295 hours using an internal mercury permeation source. For more information on the 2537
296 and 1130/1135 systems see [Landis et al. \(2002\)](#) and [Steffen et al. \(2008\)](#).

Formatted: Font color: Text 1

Formatted: Font color: Text 1

Formatted: Font color: Text 1

Deleted:

Formatted: Font color: Text 1

Formatted: Font color: Text 1

Formatted: Font color: Text 1

Formatted: Font color: Text 1

299 GEM fluxes were measured using the methods outlined in Edwards et al. (2005). Air
300 samples were drawn at heights of 5.2 and 8.0 m through 46.4 m of nylon tubing using
301 a PTFE diaphragm pump operating at 10 L min⁻¹. Subsampling from this flow through
302 a 0.2 µm PTFE filter at 1 L min⁻¹ by a Tekran 2537A, and switching between sample
303 intakes, allowed resolution of a GEM gradient every 30 minutes. The transfer velocity
304 was measured using a Campbell Scientific CSAT3 sonic anemometer and LI-COR
305 7200 closed path infrared gas analyser for CO₂, both located on the same tower as the
306 gradient intakes at 6.6 m and sampling at 20 Hz.

307 Radon

308 In order to measure Radon concentrations, a 700 L dual-flow-loop two-filter radon
309 detector, designed and built by the Australian Nuclear Science and Technology
310 Organisation (Whittlestone and Zahorowski, 1998; Chambers et al., 2014), was installed
311 at the ATARS in 2011 and has been fully operational since July 2012. The detector
312 provided continuous hourly radon concentrations for the duration of the SAFIRED
313 campaign, sampling air at 40 L min⁻¹ from 12 m above ground level through 25 mm
314 high-density polyethylene agricultural pipe. A coarse aerosol filter and dehumidifier
315 were installed “upstream” of the detector, as well as a 400 L delay volume to ensure
316 that thoron (²²⁰Rn, half-life 55 s) concentrations in the inlet air stream were reduced to
317 less than 0.5 % of their ambient values. The detector’s response time is around 45
318 minutes, and the lower limit of detection is 40 - 50 mBq m⁻³. Calibrations are performed
319 on a monthly basis by injecting radon from a PYLON 101.15±4% kBq Ra-226 source
320 (12.745 Bq min⁻¹ ²²²Rn), traceable to NIST standards, and instrumental background is
321 checked every 3 months. In post processing, half-hourly raw counts were integrated to
322 hourly values before calibration to activity concentrations (Bq m⁻³).

Formatted: Font color: Text 1

Formatted: Font color: Text 1

Formatted: Heading 3

Deleted: .

[6]

Formatted: Font:Not Bold, Font color: Text 1

Formatted: Font color: Text 1

Formatted: Font color: Text 1

Formatted: Font color: Text 1

Formatted: Font color: Text 1

Formatted: Font color: Text 1

Formatted: Font color: Text 1

325 [2.2.2 Aerosols](#)

326 **Aerosol Drying System**

327 An Automated Regenerating Aerosol Diffusion Dryer (ARADD) is permanently
328 installed on the roof of the laboratory containing the aerosol instrumentation for this
329 campaign. This was used in front of the aerosol manifold to continuously dry the aerosol
330 sample. The ARADD design, similar to that described by [Tuch et al. \(2009\)](#),
331 continuously conditions the aerosol sample to a relative humidity of below 40% with
332 maximum aerosol transmission efficiency. The ARADD utilizes two diffusion drying
333 columns in parallel, each containing 7 stainless steel mesh tubes of 10 mm internal
334 diameter and approximately 800 mm length, surrounded by a cavity packed with silica
335 gel. The aerosol sampled is directed into one column at a time, while the other column
336 is regenerated by an ultra-dry compressed air system. All flows are controlled by
337 software that directs sample flow and compressed air flow to the appropriate column
338 with a series of valves. The ARADD has [total suspended particulate style intake at the](#)
339 [inlet of the aerosol sample path. This is a non-size-selective stainless-steel inlet with a](#)
340 [semi-circular hat over an inverted conical funnel of variable pitch ending with a 3/4"](#)
341 [stainless-steel tube. In practise, the aerosols collected have an equivalent aerodynamic](#)
342 [diameter of 100 µm or less depending on sampling conditions. The inlet led to a sample](#)
343 manifold at the exit of the system to provide sampling take-offs for the various aerosol
344 instruments connected to the ARADD. Flow through the ARADD is provided by the
345 instruments and pumps connected downstream. The ambient and inlet relative humidity
346 for the entire sampling period were logged and are displayed in Supplementary Figure
347 [S1](#).

Formatted: Font color: Text 1

Formatted: Font color: Text 1

Formatted: Font color: Text 1

Formatted: Font color: Text 1

Deleted: a T

Formatted: Font color: Text 1

Deleted: S

Formatted: Font color: Text 1

Deleted: P

Formatted: Font color: Text 1

Formatted: Font color: Text 1

Deleted: , and a

Formatted: Font color: Text 1

Formatted: Font color: Text 1

352 **Aerosol Size**

353 Aerosol size distributions were measured with a Scanning Mobility Particle Sizer
354 (SMPS). A TSI 3071 long-column electrostatic classifier with a TSI 3772 Condensation
355 Particle Counter (CPC) measured the size distribution over a range of 14 nm to 670 nm
356 at a scan interval of 5 minutes.

357
358 In addition to the aerosol size distributions measured by the SMPS, neutral and charged
359 aerosol particle distributions from 0.8 nm to 42 nm were measured using a Neutral
360 cluster and Air Ion Spectrometer (NAIS)(Manninen et al., 2009;Mirme et al., 2007). In
361 this study, the NAIS was set to operate in a cycle of 4 min including ion and neutral
362 particle sampling periods of 2 and 1 minute, respectively, with the remaining minute
363 being an offset period which is required to neutralize and relax the electrodes. The total
364 sampling air flow was 60 L min⁻¹, the high flow rate being used to minimize ion
365 diffusion losses and maximize the measured ion concentration sensitivity. Ion losses
366 are accounted for during post-processing of the data by the software (Mirme et al.,
367 2007).

Formatted: Font color: Text 1
Formatted: Font color: Text 1

Formatted: Font color: Text 1

Formatted: Font color: Text 1

368 **Aerosol Composition and Water Uptake**

369 PM₁ and PM₁₀ 12-hour filter samples (night and day) were collected on a TAPI 602
370 Beta plus particle measurement system (BAM). Portions of the PM₁ filters have been
371 analysed for elemental and organic carbon mass loadings using a DRI Model 2001A
372 Thermal-Optical Carbon Analyzer following the IMPROVE-A temperature protocol
373 (Chow et al., 2007b). Additional portions of the PM₁ filters were extracted in 5 ml of
374 18.2 mΩ de-ionized water and preserved using 1% chloroform. These extracts ~~have~~
375 ~~been~~ analysed for major water-soluble ions by suppressed ion chromatography and for

Formatted: Font color: Text 1
Formatted: Font color: Text 1
Deleted: will be
Formatted: Font color: Text 1

377 anhydrous sugars including levoglucosan by high-performance anion-exchange
378 chromatography with pulsed amperometric detection (Inuma et al., 2009).

379

380 Daily aerosol filters were collected using two Ecotech 3000 high-volume volumetric
381 flow controlled aerosol samplers with PM₁₀ size selective inlets. One high-volume
382 sampler was used to collect aerosols on acid cleaned Whatman 41 filters to determine
383 the soluble and total fraction of trace metals. Soluble trace metals were extracted from
384 a filter aliquot using ultra-pure water (>18.2 mΩ) leaching experiments. Total trace
385 metal concentrations were determined by digesting a second filter aliquot with
386 concentrated nitric and hydrofluoric acids. Leachates and digested solutions were
387 analysed by high resolution inductively couple plasma mass spectrometry. The second
388 sampler was used to collect a set of aerosol samples on quartz filters for elemental and
389 organic carbon analysis following (Chow et al., 2007a) and major anion and cation
390 analysis.

391

392 The volatility and hygroscopicity of 50 nm and 150 nm particles were measured with a
393 custom built Volatility and Hygroscopicity Tandem Differential Mobility Analyser
394 (VH-TDMA). Inlet dried particles were size selected (alternating between 50 and 150
395 nm) using a TSI 3080 electrostatic classifier. Scans alternated between two different
396 sample pathways. In the first, after size selection, particles were passed through a
397 thermodenuder set to 120°C. The sample line was then split so that half went to an
398 SMPS comprised of a TSI 3080 classifier and a TSI 3010 CPC (V-TDMA). The rest of
399 the sample was passed through a humidifying system that exposed the particles to a
400 relative humidity of 90% before being brought into another SMPS with a 3080 classifier
401 and 3010 CPC (H-TDMA). Alternatively, the thermodenuder was bypassed in every

Formatted: Font color: Text 1

Formatted: Font color: Text 1

Formatted: Font color: Text 1

Formatted: Font color: Text 1

Formatted: Font color: Text 1

402 second scan so that the V-TDMA was used to verify the size selection and the H-TDMA
403 was able to observe the hygroscopic growth of ambient particles. Each scan ran for 3
404 minutes, giving a full set of data every 12 minutes.

405

406 The chemical composition and properties of non-refractory sub-micron particles were
407 investigated with a compact Time-of-Flight Aerosol Mass Spectrometer (cToF-AMS,
408 Aerodyne Research, Inc.) and a Time of Flight Aerosol Chemical Speciation Monitor
409 (ToF-ACSM, Aerodyne Research, Inc.). Both of these instruments operate with the
410 same principle and have many identical components. An aerodynamic lens in the inlet
411 of each instrument focuses the particles into a beam and differential pumping removes
412 most of the gas phase. Particles are flash vaporized at 600°C and ionized by electron
413 impact before passing through a time-of-flight mass spectrometer to a multi-channel
414 plate detector in the cToF-AMS and a dynode detector in the ToF-ACSM. The cToF-
415 AMS has the added benefit of having a particle Time-of-Flight (pToF) mode, which
416 allows the size resolved chemical composition to be measured. Both instruments
417 sampled through a PM_{2.5} inlet and nafion dryer. In addition, the inlet of the cToF-AMS
418 was incorporated into the VH-TDMA system, so that when the VH-TDMA was
419 measuring ambient particles, the cToF-AMS would draw particles through the
420 thermodenuder set at 120°C and vice-versa. This gives additional information about the
421 chemical composition of the volatile component of submicron particles.

422

423 The number of particles activated to cloud droplets were measured using a Continuous-
424 Flow Steam Wise Thermal Gradient Cloud Condensation Nuclei Counter (CCNC) from
425 Droplet Measurement Technologies Inc. (DMT, model No. 100). Particles were

426 exposed to a 0.5% supersaturation and activated particles greater than 1µm were
427 counted with an Optical Particle Counter using a 50 mW, 658 nm laser diode.

428 **Back trajectories**

429 Hourly 10-day air mass back trajectories terminating at ATARS were produced using
430 the NOAA HYSPLIT model (Draxler and Rolph, 2003), and catalogued in a data base
431 for use with the SAFIRED campaign data set. Global Data Assimilation System input
432 files with 0.5° resolution were obtained from NOAA ARL FTP site
433 (<http://ready.arl.noaa.gov/gdas1.php>) to drive the HYSPLIT model.

Formatted: Font color: Text 1

Formatted: Font color: Text 1

Formatted: Default Paragraph Font, Font color: Text 1

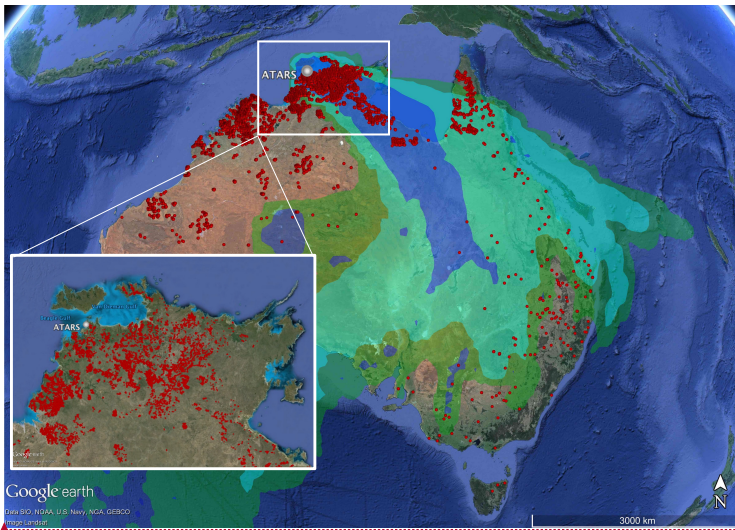
Formatted: Font color: Text 1

434 **Satellite detection of fires**

435 Data on the location of fires was collected from the Australian national bushfire
436 monitoring system, Sentinel Hotspots. Hotspot locations are derived from the Moderate
437 Resolution Imaging Spectroradiometer (MODIS) sensors on the Terra and Aqua
438 satellites and the Visible Infrared Imaging Radiometer Suite (VIIRS) sensor on the
439 Suomi NPP satellite. The Terra, Aqua and Suomi NPP satellites fly over the region
440 around ATARS at approximately 10:30 am, 3 pm and 2:30 pm, respectively. Detection
441 of fires is therefore limited to those that are flaming during these times.

442 **3. Overview of Campaign**

443 **Fires and air masses**



444
445 **Figure 1** All satellite-detected fires with >50% detection confidence in June 2014 in Australia. Trajectory
446 densities are shown as shaded regions (blue - >10% of all data; cyan - >1% of all data; green - >0.1% of all
447 data).

448 Thousands of fires were observed in during the period of the SAFIRED campaign in
449 Australia by the MODIS and VIIRS sensors on the Terra and Aqua NASA satellites.
450 The vast majority of these occurred in the savannah regions of northern Australia. Over
451 28000 fires were detected within 400 km of ATARS during the sampling period. .
452 Airmass back trajectories from the sampling site show that air masses over the study
453 period predominately originated from the southeast (see Figure 1), generally over the
454 regions where fires were frequently detected. Considering the daily satellite
455 observations of close and distant fires, as well as meteorological, gaseous and aerosol
456 measurements over the duration of SAFIRED, five periods were distinguished; four
457 biomass burning related periods (BBP1, BBP2, BBP3 and BBP4) and a "coastal" period
458 (CP). The dates for these periods are displayed in Table 2.

Formatted: Font color: Text 1

Formatted: Heading 2

Formatted: Font color: Text 1

Formatted: Font color: Text 1

Formatted: Centered

Formatted: Font color: Text 1

Deleted: The HYSPLIT (a) back and (b) forward trajectories to and from the ATARS site, truncated to five days. The colour scale represents the air mass trajectory density, normalised to 1. Grey dots are MODIS and VIIRS detected hotspots from the 30th of May 2016 until the 29th of June 2016.

Formatted: Font color: Text 1

Formatted: Font color: Text 1

Deleted: (Figure 1)

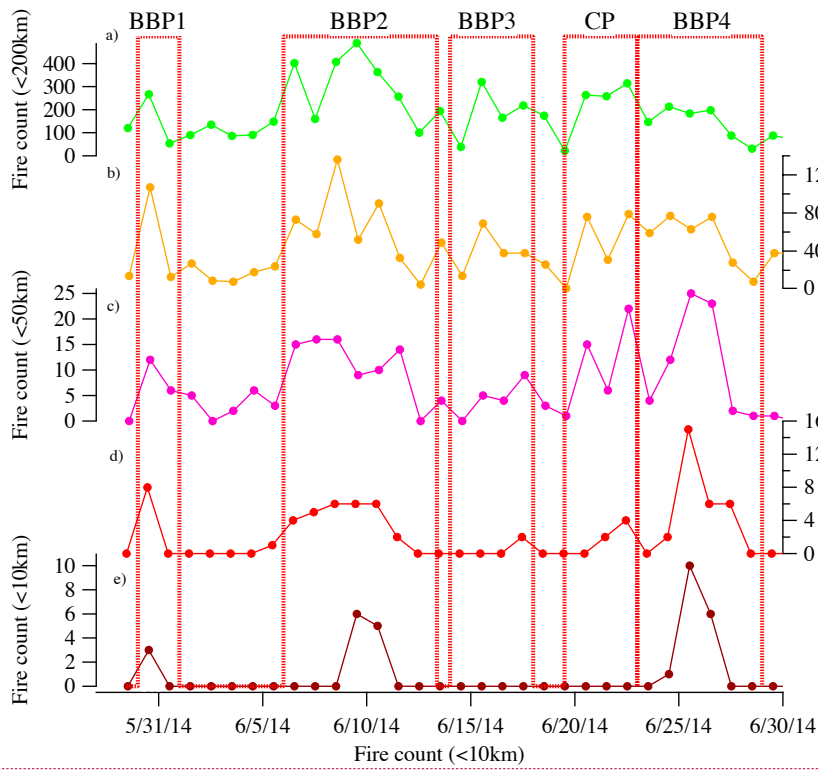
466 **Table 2** The start and end dates for the four identified Biomass Burning Periods (BBP1, BBP2, BBP3 and
 467 BBP4) and the Coastal Period (CP).

<u>Period</u>	<u>Start date (mm/dd/yy hh:mm)</u>	<u>End date (mm/dd/yy hh:mm)</u>
<u>BBP1</u>	<u>05/30/14 00:00</u>	<u>05/31/14 23:59</u>
<u>BBP2</u>	<u>06/06/14 00:00</u>	<u>06/12/14 23:59</u>
<u>BBP3</u>	<u>06/14/14 00:00</u>	<u>06/17/14 23:59</u>
<u>CP</u>	<u>06/19/14 12:00</u>	<u>06/22/14 23:59</u>
<u>BBP4</u>	<u>06/23/14 00:00</u>	<u>06/28/14 23:59</u>

468
 469 The number of detected fires on each day within 10 km, 20 km, 50 km, 100 km and 200
 470 km of the sampling location was determined (see Figure 2). Several fires within 10 km
 471 were detected on the 30th of May (BBP1), the 9th and 10th of June (BBP2) and the
 472 25th and 26th of June (BBP4). BBP1, BBP2 and BBP4 were also associated with the
 473 highest concentrations of most of the measured gaseous (Figure 3) and aerosol species
 474 (Figure 4). The periods between the 12th and 23rd of June (BBP3 and CP) had very
 475 few detected fires within 50 km of the station, corresponding to smaller gaseous and
 476 aerosol concentrations.

Deleted: The number of detected fires on each day within 10 km, 20 km, 50 km, 100 km and 200 km of the sampling location was determined (Figure 2). Several fires within 10km were detected on the 30th of May and the 9th, 10th, 25th and the 26th of June. These correspond with the highest gaseous and aerosol signals. The periods between the 11th and 24th of June had very few detected fires within 50km of the station. Satellite flyby times were in the early afternoon local time each day and therefore fires not occurring during these times would not be recorded. Airmass back trajectories from the ATARS site show that air masses over the study period were predominately southeasterly (Figures 1a and 4c), generally over the regions where fires were frequently detected.

Formatted: Font color: Text 1



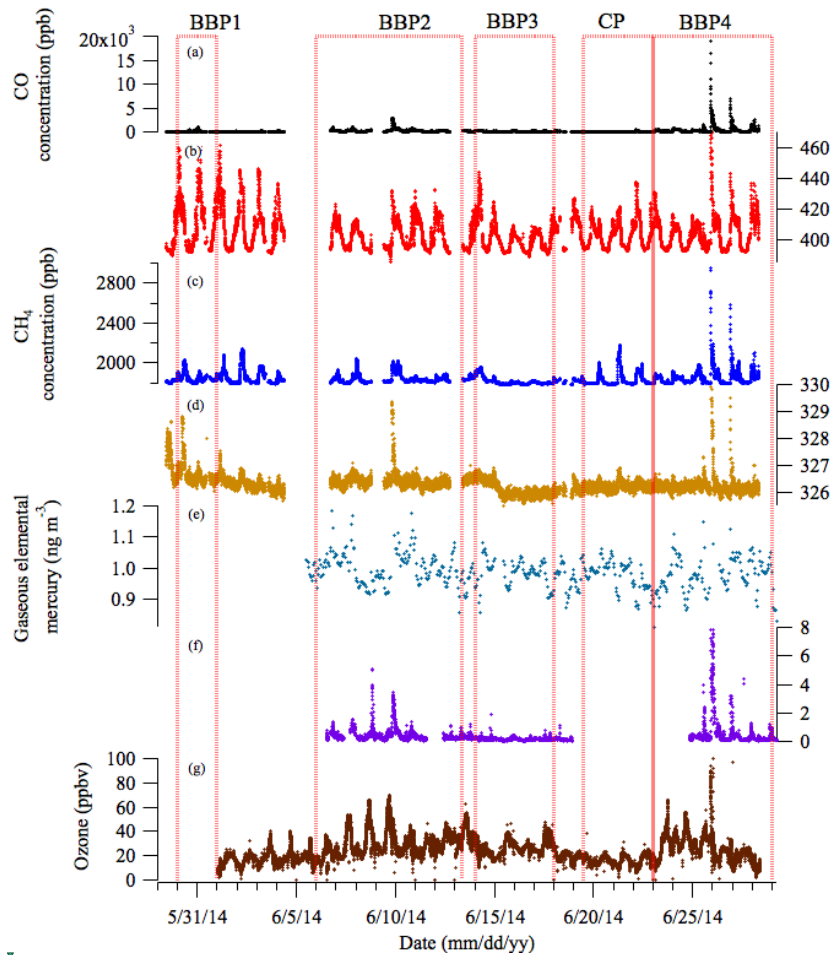
Formatted: Font color: Text 1

Formatted: Font color: Text 1

492

493
494

Figure 2 The number of hotspots observed each day within (a) 200 km, (b) 100 km, (c) 50 km, (d) 20 km and (e) 10 km of the ATARS, as detected by the MODIS and VIIRS sensors on the Terra and Aqua satellites.



Moved (insertion) [1]

Formatted: Font color: Text 1

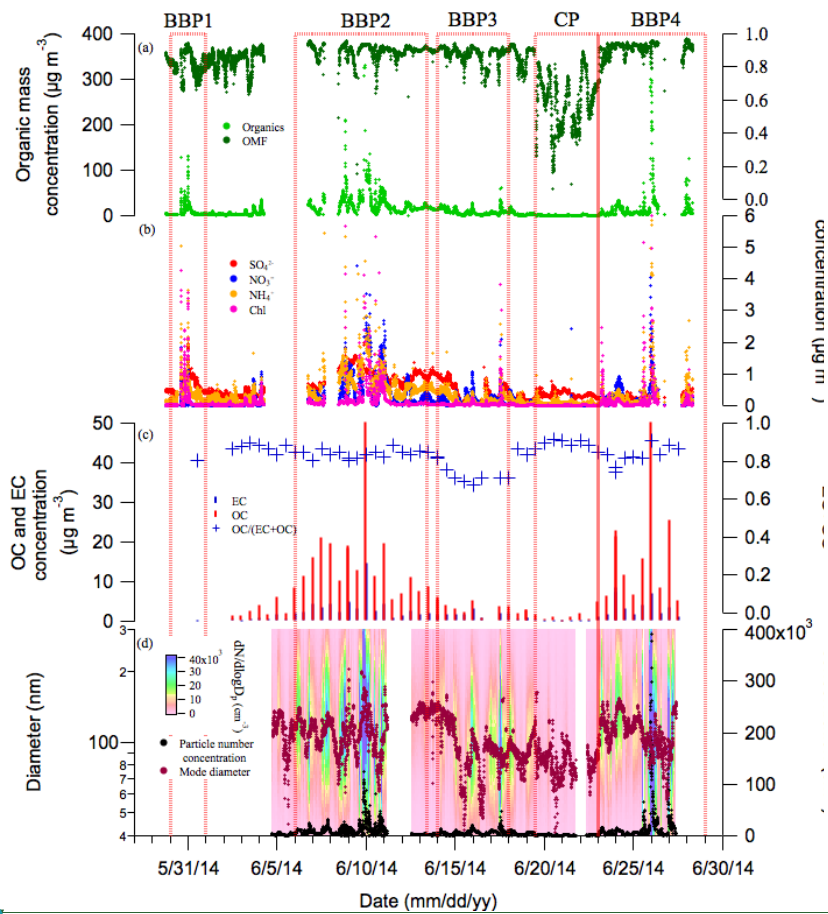
Deleted: gen

Deleted: di

Deleted: and $\Delta O_3/\Delta CO$

495

496 **Figure 3** The time series of the major measured gaseous species during the SAFIRED campaign: (a) carbon
 497 monoxide, (b) carbon dioxide, (c) methane, (d) nitrous oxide, (e) gaseous elemental mercury, (f) acetonitrile
 498 and (g) ozone. The biomass burning and coastal periods are indicated by the red dotted lines. All parts-per
 499 notation refer to mole fractions unless otherwise indicated. The date and time is local time.



Moved (insertion) [2]

Formatted: Font color: Text 1

Formatted: Caption

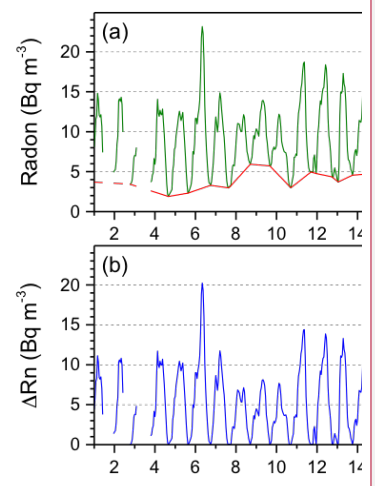
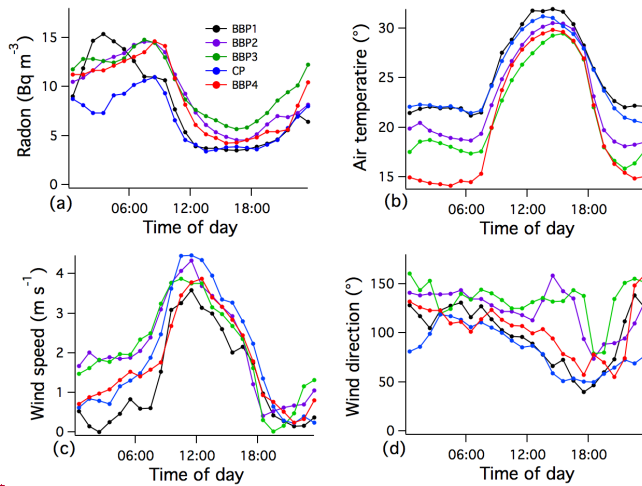
Deleted: .

[7]

Figure 4 The time series of the major aerosol properties during the SAFIRED campaign: (a) the non-refractory PM₁ organic mass concentration (left) and organic mass fraction (right), (b) the inorganic non-refractory PM₁ mass concentrations, (c) the 12-hour filter OC and EC PM₁ mass concentrations (left) and the ratio of OC to OC+EC (right), (d) the particle size distributions and particle size mode (left) and the total particle number concentration (right) and (e) the wind direction at ATARS. The date and time is local time.

Most of the gaseous and aerosol time series show a pronounced diurnal trend, with higher concentrations typically observed during the night (see Supplementary Figures S2 and S3). This is likely due to a combination of variations in fire locations, time of burns, and changes in the boundary layer height or wind velocity. The diurnal trends of radon concentrations, temperature, wind speed and wind direction for each of the BBPs and the CP are displayed in Figure 5. The radon concentrations provide further

517 [information regarding the regional air mass origins and the degree of contact with the](#)
518 [land surface and give insight into the boundary layer. Sharp decreases in the radon](#)
519 [concentrations were observed after 09:00 local time and did not increase until after](#)
520 [sunset at approximately 18:00 for all periods \(Figure 5a\), suggesting a pronounced](#)
521 [diurnal variation in the boundary layer height. Furthermore, radon concentrations were](#)
522 [consistently lower during the CP than the BB periods, suggesting less terrestrial](#)
523 [influence than the rest of the sampling period. The HYSPLIT air mass back trajectory](#)
524 [for the CP originated along the east coast of Australia and passing over little land before](#)
525 [arriving at the station. Figure 5d supports this, showing predominately easterly and](#)
526 [northeasterly winds during the night and day, respectively. The diurnal variations](#)
527 [during the BB periods were more pronounced. The winds during these periods were](#)
528 [predominately southeasterly during the night and morning, turning easterly during the](#)
529 [afternoon before reverting at approximately 20:00 local time. The HYSPLIT air mass](#)
530 [back trajectories for the BB periods indicated terrestrial origins, with air masses passing](#)
531 [predominately over the savannah region of northern Australia where the fires occurred.](#)



Deleted: ... [8]

Formatted: Font color: Text 1

Formatted: Font color: Text 1

Formatted: Font color: Text 1

Formatted: Font color: Text 1

Formatted: Centered

Formatted: Font color: Text 1

Formatted: Font color: Text 1

Formatted: Font color: Text 1

Formatted: Font color: Text 1

Formatted: Font color: Text 1

Deleted: 4

Formatted: Font color: Text 1

Deleted: composite

Deleted: as a function of radon-based nocturnal mixing categories.

Formatted: Font color: Text 1

532

533 **Figure 5** Mean hourly diurnal (a) radon, (b) wind speed, (c) wind direction, and (d) dew point temperature at

534 ATARS, separated into different biomass burning periods (BBP) and a coastal period (CP).

535 [With numerous fires occurring across the region and the limitations of once-per-day](#)

536 [satellite fly-overs and stationary measurements, it can be difficult to identify the exact](#)

537 [source of these elevated signals. Nonetheless, it is possible to link detected plumes with](#)

538 [fires given back trajectory analysis. The elevated signals during BBP1 were likely a](#)

539 [result of several fires that were burning and observed on the 30th of May at 14:00 local](#)

540 [time approximately 2 and 10 km from ATARS during the day. While the elevated](#)

541 [signals were observed later in the evening, it is likely that they were due to a](#)

542 [continuation or evolution of those fires. Some of the most intense signals of the](#)

543 [campaign were observed during BBP2, with numerous close \(within 50 km\) and distant](#)

544 [\(within 200 km\) detected. Due to the limitations of the once-per-day satellite fly-by, it](#)

545 [was only possible to link one of the observed plumes to a source during this period. A](#)

546 [large event observed on the evening of the 9th of June was likely due to a cluster of](#)

547 [fires detected approximately 5 km southeast of ATARS. Only one fire within 20 km of](#)

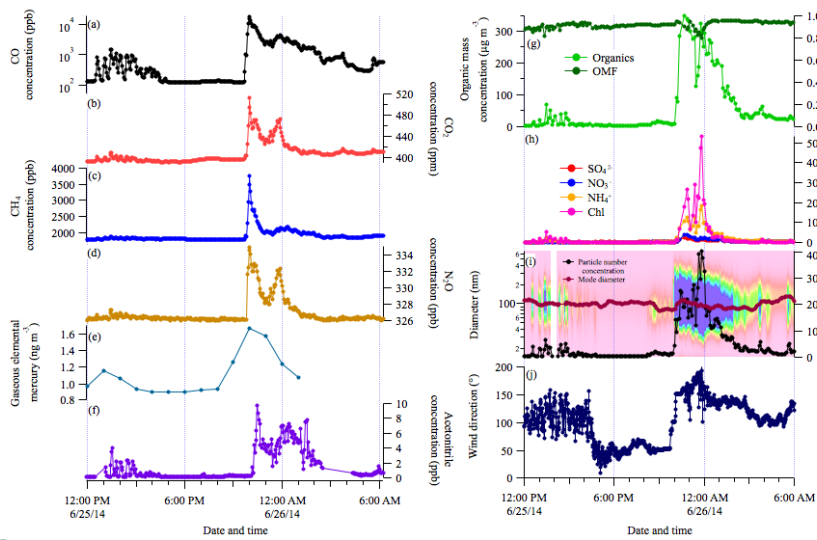
548 [ATARS was observed via satellite during BBP3 on the 17th of June but this was not](#)

555 associated with any significant increase in gaseous or aerosol concentrations. Several
556 fires were also observed between 20 km and 50 km from the station. One close fire was
557 also observed during CP, however wind directions during this period were typically
558 north-easterly and concentrations were therefore much lower. 5-day HYSPLIT
559 trajectories also show that air mass during the CP originated along the east coast of
560 Australia before travelling towards the sampling station with very little terrestrial
561 influence.

Formatted: Font color: Auto

562
563 For a portion of BBP4, fires were burning within several kilometers of ATARS and
564 several plumes were easily observed from the station. The signals from these plumes
565 are shown in Figure 6. The observed enhancements between 12:30 and 15:00 pm on
566 the 25th June during BBP4 were a result of grass fires burning approximately 2 km
567 south-east from the station. During this event, the wind direction was highly variable,
568 changing between 140° and 80° True Bearing (TB) multiple times. As a result, the
569 sampling changed from measuring the air mass with and without the plume from this
570 fire, which led to sharp increases and decreases in biomass burning-related signals.
571 Visually, the fire area and extent of the plume was larger at 4:00pm than earlier,
572 however the wind direction changed to north-easterly which directed the plume away
573 from the station. From 16:00 until 22:00, the wind direction was stable at
574 approximately 50° TB. At 22:00, the wind direction rapidly changed to directly south
575 and the largest enhancements for the whole campaign were observed until
576 approximately 2:00 am on the 26th of June. It is very likely that these signals were a
577 result of a continuation and evolution of these fires as the night progressed. Portions of
578 a ~0.25 km² grassland field within 500 m directly south of ATARS were observed to
579 be burned upon arrival at the station on the morning of the 26th of June and we speculate

580 [that the burning of this field contributed to the large enhancements in measured biomass](#)
 581 [burning emissions. The emissions during this portion of BBP4 are likely to be the most](#)
 582 [representative of fresh biomass burning smoke during the SAFIRED campaign.](#)
 583 [Significant ozone enhancements over 80 ppb were observed during this event, although](#)
 584 [this was likely result of a cross-contamination due to concurrently high concentrations](#)
 585 [of UV-absorbing organic compounds in the gaseous phase. This enhancement would](#)
 586 [only be possible with significant photochemical processing which is very unlikely](#)
 587 [considering the time of the event, the visual evidence of close fires, and the large](#)
 588 [concentrations observed.](#)



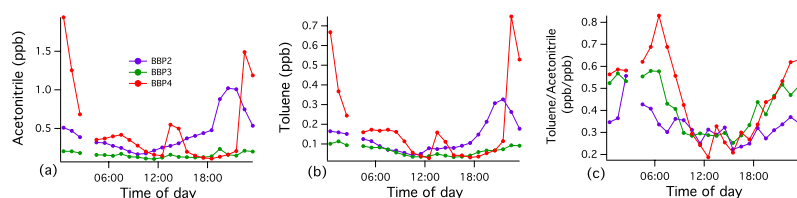
Moved (insertion) [3]
 Formatted: Font color: Text 1

589 **Figure 6.** The major gas and aerosol concentrations measured during two biomass burning events within 1
 590 km of ATARS during BBP4. (a) through (g) and (h) through (k) are as per Figures 3 and 4, respectively. All
 591 parts-per notation or mole fractions unless otherwise indicated. The date and time are local time.

Deleted: 8
 Deleted: 5
 Deleted: 6

593 [Based on the elevated concentrations of biomass burning related gaseous and aerosol](#)
 594 [species, detection of close fires and the air mass back trajectory analysis during portions](#)
 595 [of BBP1, BBP2 and BBP4, these periods are likely associated with fresh biomass](#)
 596 [burning smoke from nearby fires. With smaller concentrations and more distant](#)

600 observed fires, the signals observed during BBP3 are possibly more characteristic of
601 aged biomass burning smoke. The influence of biomass burning during CP was much
602 smaller than the rest of the campaign. Investigating the relationship between toluene
603 and acetonitrile, two NMOCs emitted from biomass burning, can provide further
604 information on the aging of BB emissions. Toluene is much shorter lived than
605 acetonitrile as it readily reacts in the presence of the OH radical. Assuming a consistent
606 emission ratio of these two NMOCs from fires in this region, the ratio of
607 toluene/acetonitrile thereby provides a proxy for photochemical age. Unfortunately, the
608 PTR-MS which measures these species was not operational during BBP1 and CP. The
609 diurnal trends for the toluene and acetonitrile concentrations and the
610 toluene/acetonitrile ratio is shown in Figure 7 for BBP2, BBP3 and BBP4. The
611 toluene/acetonitrile ratio was highest during the night, indicating more photochemically
612 aged smoke throughout the day. Interestingly, while the toluene and acetonitrile
613 concentrations were consistently higher during BBP2 and BBP4 than BBP3, the
614 toluene/acetonitrile ratio was of the same magnitude and followed the same trend. It is
615 therefore plausible that, while there were not large enhancements in concentrations
616 during BBP3 and there were few fires detected close-by during the daytime satellite
617 flyovers, there were small-scale burns during the night that were close enough for the
618 emissions to reach sampling site. This observation highlights the limitation of using
619 satellite hotspot detection in fully understanding the aging processes of biomass
620 burning emissions.



Formatted: Font color: Text 1

621

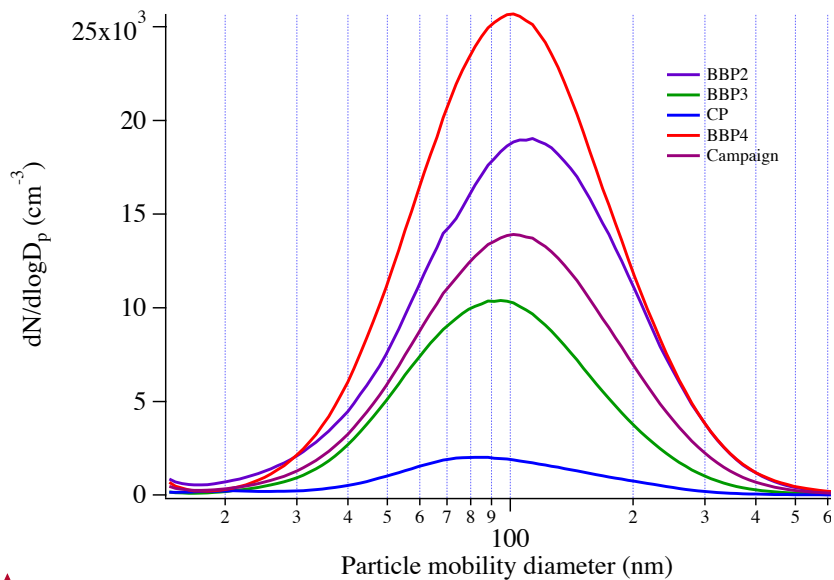
622 Figure 7 Mean hourly diurnal (a) acetoneitrile concentration, (b) toluene concentration, (c) toluene/acetoneitrile
 623 ratio, separated into different biomass burning periods (BBP).

Formatted: Caption

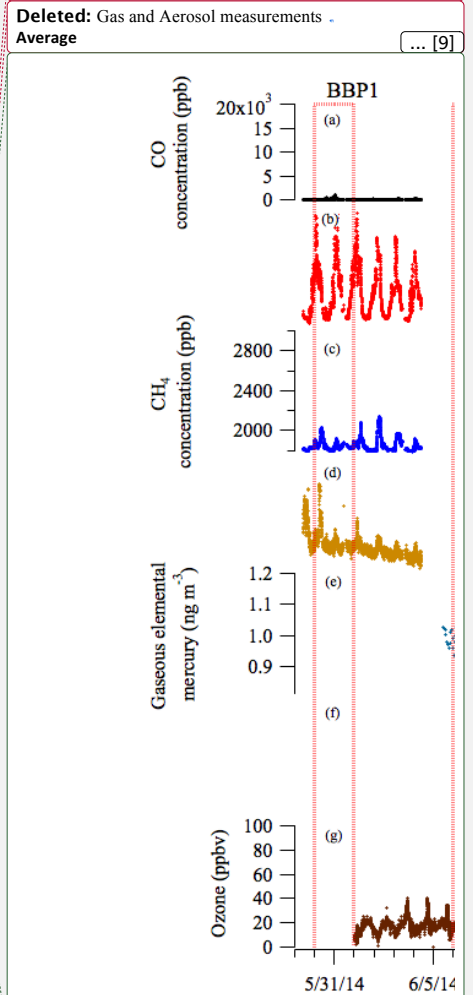
624

625 Particle size distributions were unimodal for the majority of the sampling period with
 626 a mode of approximately 100 nm on average (see Figure 8). The SMPS was not
 627 operational during BBP1. Although the shape of the BBP4 size distribution was similar
 628 to the campaign average, concentrations were much higher and a result of close fires.
 629 BBP2 had a slightly larger size distribution centered on 110 nm. The size distribution
 630 during BBP3 was slightly smaller than the campaign average and BBP2 and BBP4,
 631 with a mode centered on ~95 nm. Furthermore, the diurnal trends of the BBA mode
 632 diameter during BBP2, BBP3 and BBP4 and CP all showed a clear maximum during
 633 the night (see Supplementary Figure S3d). The diurnal trends of the toluene/acetoneitrile
 634 ratios (Figure 7c) as well as the ratio of oxygenated organic aerosol to total organics
 635 (see Supplementary Figure S3c) suggest that the larger night time particle sizes are
 636 more associated with fresh biomass burning. The contrast between these size
 637 distributions could be a result of atmospheric aging and dilution in which organic mass
 638 condenses onto or evaporates from the particle. Variations in fuel load or burning
 639 conditions could also contribute to this difference. The size and concentration of
 640 particles during the Coastal Period (CP) were much smaller than the rest of the
 641 campaign. There were two periods during CP where a bimodal size distribution was
 642 observed; one from approximately 3 pm until midnight on the 19th of June and the other
 643 between 2 pm and 6 pm on the 20th of June. The size distributions for both of these

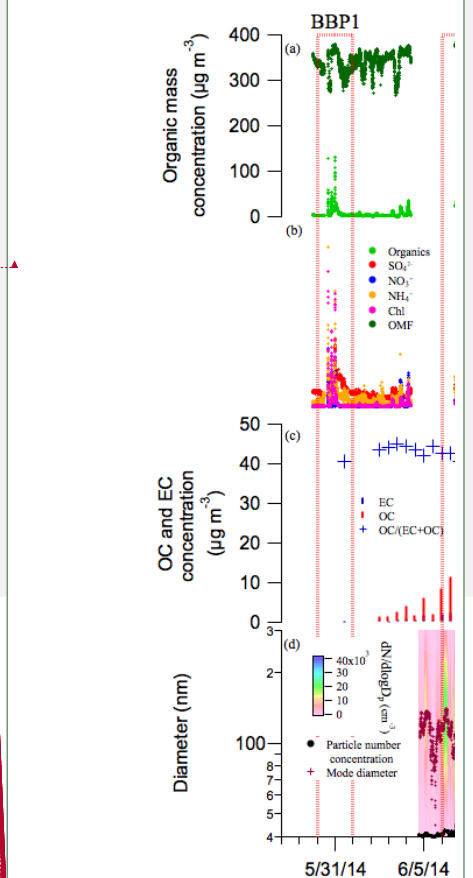
644 periods had a mode at approximately 20 nm and another at approximately 85 nm.
 645 Submicron sulfates made up to 32% of the total submicron non-refractory mass
 646 concentrations, as reported by the cToF-AMS from the period of midday on the 19th of
 647 June until midnight on the 22nd of June, whereas the average sulfate contribution for
 648 the rest of the campaign was approximately 8%. The low radon values, small particle
 649 concentrations, bimodal size distributions and significant contributions of sulfate
 650 during this period also suggest very little biomass burning signal and a more marine-
 651 like aerosol. No particle nucleation events were observed over the entire sampling
 652 period (See Supplementary Figure S4). This is likely due to the elevated particle
 653 concentrations acting as a condensation sink.



657 **Figure 8** The average number size distribution during BBP2, BBP3, BBP4, CP and the campaign average.
 658 Over the campaign, organics dominated the non-refractory sub-micron aerosol mass
 659 contributing, on average, 90% of the total mass. Sulphate, nitrates, ammonium and
 660



Moved up [11]: [14]



Moved up [21]: [16]

Formatted [10]

Formatted [11]

Formatted [12]

Formatted [13]

Formatted: Font color: Text 1 [15]

Formatted [15]

Formatted [17]

chloride species contributed the rest of this mass, with the largest contributions from sulphate and ammonium. Sulphate contributions were very significant during the coastal period, contributing up to 32% of the total mass. Although chlorides contributed the least to the total mass on average, during clear biomass burning events where sharp increases in CO and organics were observed, chlorides made up the largest component of inorganic aerosol. Organic carbon made up approximately 80% to 90% of the total carbon (organic carbon + elemental carbon) PM₁ mass during the campaign, with the exception of BBP3, when this dropped to 70%. Whether these observations were a result of burn conditions or aging processes (i.e. evaporation of organic compounds from the aerosol phase) is unclear.

4. Outcomes of SAFIRED

The overall aim of this study was to investigate the characteristics of BB emissions in the tropical savannah region of northern Australia during the early dry season. For many gaseous and aerosol species, elevated signals were observed for much of the month-long sampling period due to the high frequency of fires. Further analysis of these species can provide more insight into the impact of these fires on the regional atmosphere. Table 2 displays a summary of companion studies undertaken within the SAFIRED campaign.

Table 3 A list of currently published companion studies undertaken during SAFIRED.

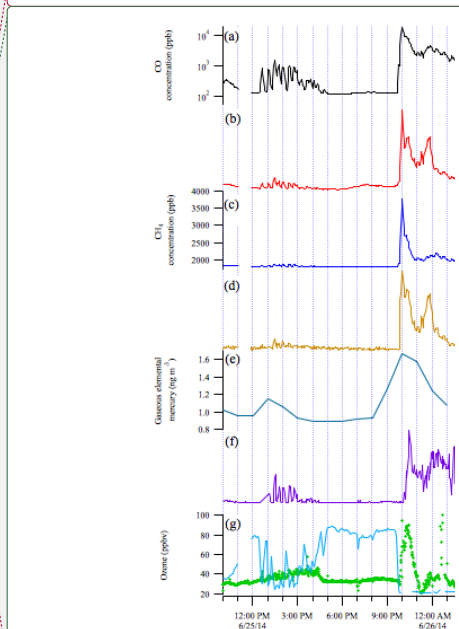
Reference	Title
Winton et al., (2016)	Dry season aerosol iron solubility in tropical northern Australia

Formatted: Subscript

Formatted: Font color: Text 1

Deleted: BBP1, BBP2 and BBP4 correspond to the periods when fires were burning within 10 km of ATARS. Large enhancements of biomass burning related emissions were observed during these three periods. There were distinct enhancements of all measured gaseous and aerosol species during these periods. Differences between the maximum and background concentrations were very prominent for CO (note the logarithmic scale in Figure 5a), CH₄, N₂O, ... [19]

Formatted: Font color: Text 1



Moved up [3]:

Formatted: Font color: Text 1, Superscript

Formatted: Font color: Text 1

Deleted: (i.e. evaporation of organic compounds from the aerosol phase) is unclear, although the highest ΔO₃/Δ... [20]

Formatted: Font color: Text 1

Formatted: Font:Not Bold, Font color: Text 1

Formatted: Font color: Text 1

Formatted: Font:Bold, Font color: Text 1

Formatted: Font color: Text 1

Formatted: Font color: Text 1

Formatted: Font color: Text 1

Formatted: Font color: Text 1

Formatted: Font color: Text 1

Formatted: Font color: Text 1

Formatted: Caption, Keep with next

Formatted Table

[Wang et al., \(2017\)](#) [Emissions of selected semivolatile organic chemicals from forest and savannah fires](#)

[Milic et al., \(2017\)](#) [Biomass burning and biogenic aerosols in northern Australia during the SAFIRED campaign](#)

[Mallet et al., \(2017\)](#) [Composition, size and cloud condensation nuclei activity of biomass burning aerosol from northern Australian savannah fires](#)

[Desservattaz et al., \(2017\)](#) [Emission factors of trace gases and particles from tropical savanna fires in Australia](#)

[Howard et al., \(2017\)](#) [Atmospheric mercury in the southern hemisphere tropics: seasonal and diurnal variations and influence of inter-hemispheric transport](#)

751

752

753

754

755

756

757

758

759

760

761

762

763

[4.1. Emission factors and gaseous species loadings](#)

[Desservattaz et al., \(under review\)](#) identified individual plumes with high signals during SAFIRED in order to determine emissions factors CO₂, CO, CH₄, N₂O, as well as GEM, Aitken and Accumulation mode aerosols and submicron non-refractory particle species (organics, sulfates, nitrates, ammonium and chlorides). Seasonal emission factors for the major greenhouse gases are important for national greenhouse gas inventories and in understanding the impact of savannah fires. Furthermore, these results will be the first set of emission factors for aerosol particles from savannah fires in Australia, with early results suggesting higher factors than those observed from African and South American savannah fires. Emission factors were mostly found to be dependent on the combustion conditions (using the modified combustion efficiency as a proxy) of the fires.

Deleted: The more specific outcomes of SAFIRED are outlined below.

Formatted: Font color: Text 1

Formatted: Font color: Text 1

Formatted: Font color: Text 1

Formatted: Heading 2

766
767 Wang et al. (2017) investigated 13 major PAH compounds in both the gaseous and
768 aerosol phase during the SAFIRED campaign and estimated their emission factors from
769 savannah fires, as well as for subtropical eucalypt forest fires. Concentrations of these
770 PAHs varied from from ~ 1 to over 15 ng m^{-3} within different BB periods and the
771 emission factor for savannah fires for Σ_{13} PAHs were estimated to be $1600 \pm 110 \mu\text{g}$
772 kg^{-1} . In the gas phase, 3- and 4-ring compounds typically contributed $\sim 90\%$ to the sum
773 concentrations whereas the particle-associated PAHs were dominated by 5- and 6-ring
774 compounds ($> 80\%$). Measured PAH concentrations were significantly higher during
775 BBP2 and BBP4. During these periods, concentrations of BaP exceeded the monitoring
776 investigation level for atmospheric BaP (0.30 ng m^{-3}) in Australia (National-
777 Environment-Protection-Council-Service-Corporation, 2011) by up to 200%.

778
779 Biomass burning produces significant amounts of semi-volatile NMOC which can be
780 difficult to quantify and identify with current measurement techniques. However recent
781 studies have shown that including semi volatile NMOC chemistry in models improves
782 the agreement between the modeled and observed organic aerosol (Alvarado et al.,
783 2015; Konovalov et al., 2015) and ozone (Alvarado et al., 2015). High quality NMOC
784 emission factors are crucial for models to assess the impact of biomass burning plumes
785 on air quality and climate. Future analyses will be undertaken on the SAFIRED data to
786 quantify emission factors for various NMOCs.

787
788 SAFIRED represents the first measurements of atmospheric mercury undertaken in the
789 tropical region of the Australian continent. The mean observed GEM concentration
790 over the study period was $0.99 \pm 0.09 \text{ ng m}^{-3}$, similar to the average over that month

852 comprising 47% and 29%, respectively. These results indicate the significant influence
853 of fresh and aged BB on aerosol composition in the early dry season. The emission of
854 precursors from fires is likely responsible for some of the SOA formation.

855
856 The water uptake of aerosols during SAFIRED was further investigated in Mallet et al.,
857 (2017) to identify the influence of early dry season BB in this region on cloud
858 formation. The concentrations of cloud condensation nuclei at a constant
859 supersaturation of 0.5% were typically of the order of 2000 cm⁻³ and reached well over
860 10000 cm⁻³ during intense BB events. Variations in the ratio of aerosol particles
861 activating cloud droplets showed a distinct diurnal trend, with an activation ratio of
862 40% ± 20% during the night and 60% ± 20% during the day. The particle size
863 distribution and the hygroscopicity of the particles were found to significantly influence
864 this activation ratio. Particles were generally extremely hydrophobic, particularly
865 during the night and during the BB periods shown in this paper. Modelling CCN
866 concentrations using the size distributions of aerosols and typical continental and
867 terrestrial values of hygroscopicities yielded significant over predictions of up more
868 than 200%, highlighting the need to include more regional parameterisations of aerosol
869 composition and hygroscopicity.

870
871 Furthermore the fractional solubility of aerosol iron and other trace metals during
872 SAFIRED were investigated in Winton et al., (2016). The fractional iron solubility is
873 an important variable determining iron availability for biological uptake in the ocean.
874 On a global scale, the large variability in the observed fractional iron solubility results,
875 in part, from a mixture of different aerosol sources. Estimates of fractional iron
876 solubility from fire combustion (1 - 60 %) are thought to be greater than those

Formatted: Normal

877 [originating from mineral dust \(1 - 2%\) \(Chuang et al., 2005;Guieu et al., 2005;Sedwick](#)
878 [et al., 2007\), and may vary in relationship to biomass and fire characteristics as well as](#)
879 [that of the underlying terrain \(Paris et al., 2010;Ito, 2011\). Iron associated with BB may](#)
880 [provide information with respect to BB inputs of iron to the ocean \(Giglio et al.,](#)
881 [2013;e.g. Meyer et al., 2008\). The ATARS provides an ideal location to further](#)
882 [investigate BB derived fractional iron solubility at the source. The results from this](#)
883 [study can be found in Winton et al. \(2016\) and show that soluble iron concentrations](#)
884 [from BB sources are significantly higher than those observed in Southern Ocean](#)
885 [baseline air masses from the Cape Grim Baseline Air Pollution Station, Tasmania,](#)
886 [Australia \(Winton et al., 2015\). Aerosol iron at SAFIRED was a mixture of fresh BB,](#)
887 [mineral dust, sea spray and industrial pollution sources. The fractional iron solubility](#)
888 [\(2 - 12%\) was relatively high throughout the campaign and the variability was related](#)
889 [to the mixing and enhancement of mineral dust iron solubility with BB species.](#)

Formatted: Font color: Text 1

890 **5. Conclusions and looking forward**

891 [Biomass burning was found to significantly influence the surface atmospheric](#)
892 [composition during the 2014 early dry season in north Australia. Over 28000 fires were](#)
893 [detected via satellite retrieval during the sampling period. Several periods were](#)
894 [identified when fires within 20 km of the research station resulted in significant](#)
895 [enhancements of greenhouse gases, non-methane gaseous organic compounds, gaseous](#)
896 [elemental mercury and polycyclic aromatic hydrocarbons and aerosol loadings. Much](#)
897 [of the PM₁ mass was comprised of organic material. The aerosol particle number size](#)
898 [distributions were typically unimodal and centered around 100 nm which is smaller](#)
899 [than BBA observed in other regions. The analysis of the time series of these measured](#)
900 [quantities has so far allowed the quantification of savannah fire emission factors for](#)

Deleted: Atmospheric chemistry and radiative forcing will depend on how gaseous and aerosol emissions from fires age as they move and interact with each other and existing species in the atmosphere. Biomass burning aerosols can be involved in condensation and coagulation (Radhi et al., 2012), undergo water uptake (Mochida and Kawamura, 2004) form cloud droplets (Novakov and Corrigan, 1996), and be exposed to photochemical aging processes, including those involving the gaseous components of fire emissions (Keywood et al., 2011;Keywood et al., 2015). With a reported lifetime of 3.8 ± 0.8 days (Edwards et al., 2006), biomass burning aerosols are able to travel intercontinental distances (Rosen et al., 2000) and are therefore present in the atmosphere long enough for substantial changes due to aging. Furthermore, tropical convection is likely to affect the aging of BB emissions in the region around ATARS, due to the immediate proximity to the warm waters in the Timor Sea (Allen et al., 2008). This introduces further uncertainty to the effect of BB emissions on radiation flux. ... [24]

Deleted: L

Formatted: Font color: Text 1

Formatted: Font color: Text 1

Formatted: Font color: Text 1

922 [these aerosol and gaseous species and has provided and understanding of the aerosol](#)
923 [aging, water uptake and solubility in this region.](#)

924

925 While the specific outcomes of the SAFIRED campaign are reviewed [in the previous](#)
926 [section](#), the general importance of this study can be discussed in a greater context. This

Deleted: above

Formatted: Font color: Text 1

Formatted: Font color: Text 1

927 is the first large-scale collaborative project undertaken in this region and draws on the
928 resources and expertise of most of Australia's research institutes focused on atmosphere
929 chemistry and composition. Large scale, multidisciplinary measurement campaigns in
930 the tropics, such as SAFIRED, are needed to make distinctions between different types
931 of fires in different regions to reduce uncertainties in global climate models (Keywood
932 et al., 2013). This need has been recognized with the formation of global collaborative
933 initiatives promoting interdisciplinary collaboration in biomass burning research
934 (Kaiser and Keywood, 2015). As the world moves towards a warmer climate, [it is](#)

935 [plausible that the](#) frequency and intensity [of biomass burning will increase](#), and these
936 emissions will become an increasingly important source of trace gases and aerosols to
937 the atmosphere.

Formatted: Font color: Text 1

Deleted: biomass burning is likely to increase in

Formatted: Font color: Text 1

938

939 SAFIRED lays the foundation for future measurements at ATARS that could make
940 measurements throughout the whole dry season and on a more long-term scale. Future
941 work in this region should focus on 1) the detailed characterisation of individual fires
942 and their emissions, 2) biomass burning emissions throughout the late dry season and
943 3) the vertical and horizontal transport of biomass burning emissions in this region.

Formatted: Font color: Text 1

944 [With well-established emission factors, a concentrated effort should be made to link](#)
945 [modelled aerosol gaseous and aerosol loadings with *in situ* and remote sensing](#)
946 [measurements. This should be done not just at the surface, but throughout the boundary](#)

949 [layer as well as over the waters north of Australia. Furthermore, a further investigation](#)
950 [of the radiative influence of the gaseous and aerosol species should be done for this](#)
951 [region.](#)

952 **Data availability**

Formatted: Font color: Text 1

953 All data are available upon request from the corresponding authors (Branka Miljevic,
954 b.miljevic@qut.edu.au; Melita D. Keywood; melita.keywood@csiro.au).

955 **Author Contributions**

956 M.D. Mallet^{a,b,c,d,e}, M.J. Desservettaz^{b,c,d,e}, B. Miljevic^{b,c,e*}, A. Milic^{b,d,e}, Z.D.
957 Ristovski^{b,e}, J. Alroe^{b,c,e}, L.T. Cravigan^{b,c,e}, E.R. Jayaratne^{d,e}, C. Paton-Walsh^{b,c,e},
958 D.W.T. Griffith^{b,d,e}, S.R. Wilson^{b,d,e}, G. Kettlewell^{b,e}, M.V. van der Schoot^{b,e}, P.
959 Selleck^{b,c,d,e}, F. Reisen^{b,c,e}, S.J. Lawson^{b,c,d,e}, J. Ward^{b,c,d,e}, J. Harnwell^{b,c,e}, M.
960 Cheng^{b,c,d,e}, R.W. Gillett^{b,c,d,e}, S.B. Molloy^{d,e}, D. Howard^{b,c,d,e}, P.F. Nelson^{b,e}, A.L.
961 Morrison^{b,e}, G.C. Edwards^{b,c,e}, A.G. Williams^{b,c,e}, S.D. Chambers^{b,c,d,e}, S.
962 Werczynski^{b,c,e}, L.R. Williams^{c,d,e}, V.H.L. Winton^{b,c,d,e}, and B. Atkinson^{b,c}, X.
963 Wang^{b,d,e}, M.D. Keywood^{b,c,d,e,f*}

964 a: Wrote and organised the manuscript

965 b: Contributed to the organisation of the campaign

966 c: Installed and/or operated instrumentation during the sampling period

967 d: Analysed data

968 e: Contributed to the manuscript and/or data interpretation

969 f: Designed and led the campaign.

970 *: Corresponding author

971 **Competing interests**

972 The authors declare that they have no conflict of interest.

973 **Acknowledgements**

974 The majority of the campaign was internally funded. The input of QUT was supported
975 by the Australian Research Council Discovery (Grant DP120100126). The work on
976 aerosol iron solubility was supported by Curtin University (RES-SE-DAP_AW-47679-
977 1), the University of Tasmania (B0019024) and the Australian Research Council (Grant
978 FT130100037).

979 **6. References**

- 980 Akagi, S. K., Craven, J. S., Taylor, J. W., McMeeking, G. R., Yokelson, R. J., Burling,
981 I. R., Urbanski, S. P., Wold, C. E., Seinfeld, J. H., Coe, H., Alvarado, M. J., and Weise,
982 D. R.: Evolution of trace gases and particles emitted by a chaparral fire in California,
983 Atmospheric Chemistry and Physics, 12, 1397-1421, 2012.
- 984 Andersen, A. N., Cook, G. D., Corbett, L. K., Douglas, M. M., Eager, R. W., Russell-
985 Smith, J., Setterfield, S. A., Williams, R. J., and Woinarski, J. C.: Fire frequency and
986 biodiversity conservation in Australian tropical savannas: implications from the
987 Kapalga fire experiment, Austral Ecology, 30, 155-167, 2005.
- 988 Bindoff, N. L., Stott, P. A., AchutaRao, K. M., Allen, M. R., Gillett, N., Gutzler, D.,
989 Hansingo, K., Hegerl, G., Hu, Y., Jain, S., Mokhov, I. I., Overland, J., Perlwitz, J.,
990 Sebbari, R., and Zhang, X.: Detection and Attribution of Climate Change: from Global
991 to Regional, in: Climate Change 2013: The Physical Science Basis. Contribution of
992 Working Group I to the Fifth Assessment Report of the Intergovernmental Panel on
993 Climate Change, edited by: Stocker, T. F., Qin, D., Plattner, G.-K., Tignor, M., Allen,
994 S. K., Boschung, J., Nauels, A., Xia, Y., Bex, V., and Midgley, P. M., Cambridge
995 University Press, Cambridge, United Kingdom and New York, NY, USA, 867–952,
996 2013.
- 997 Chambers, S. D., Hong, S.-B., Williams, A. G., Crawford, J., Griffiths, A. D., and Park,
998 S.-J.: Characterising terrestrial influences on Antarctic air masses using Radon-222
999 measurements at King George Island, Atmospheric Chemistry and Physics, 14, 9903-
1000 9916, 2014.
- 1001 Chow, J. C., Watson, J. G., Chen, L. W. A., Chang, M. C. O., Robinson, N. F., Trimble,
1002 D., and Kohl, S.: The IMPROVE-A temperature protocol for thermal/optical carbon
1003 analysis: maintaining consistency with a long-term database, Journal of the Air &
1004 Waste Management Association, 57, 1014-1023, 2007a.

Formatted: Font color: Text 1, Spanish

1005 Chow, J. C., Watson, J. G., Chen, L. W. A., Chang, M. O., Robinson, N. F., Trimble,
1006 D., and Kohl, S.: The IMPROVE-A temperature protocol for thermal/optical carbon
1007 analysis: maintaining consistency with a long-term database, *Journal of the Air &*
1008 *Waste Management Association*, 57, 1014-1023, 2007b.

1009 Chuang, P. Y., Duvall, R. M., Shafer, M. M., and Schauer, J. J.: The origin of water
1010 soluble particulate iron in the Asian atmospheric outflow, *Geophysical Research*
1011 *Letters*, 32, L07813, 2005.

1012 Crutzen, P. J., and Andreae, M. O.: Biomass burning in the tropics: Impact on
1013 atmospheric chemistry and biogeochemical cycles, *Science*, 250, 1669-1678, 1990.

1014 Draxler, R. R., and Rolph, G.: HYSPLIT (HYbrid Single-Particle Lagrangian
1015 Integrated Trajectory) model access via NOAA ARL READY website ([http://www/](http://www.arl.noaa.gov/ready/hysplit4.html)
1016 [arl.noaa.gov/ready/hysplit4.html](http://www.arl.noaa.gov/ready/hysplit4.html)). NOAA Air Resources Laboratory, Silver Spring,
1017 in, Md, 2003.

1018 Du, H., Kong, L., Cheng, T., Chen, J., Du, J., Li, L., Xia, X., Leng, C., and Huang, G.:
1019 Insights into summertime haze pollution events over Shanghai based on online water-
1020 soluble ionic composition of aerosols, *Atmospheric Environment*, 45, 5131-5137, 2011.

1021 Edwards, G. C., Rasmussen, P. E., Schroeder, W. H., Wallace, D. M., Halfpenny-
1022 Mitchell, L., Dias, G. M., Kemp, R. J., and Ausma, S.: Development and evaluation of
1023 a sampling system to determine gaseous Mercury fluxes using an aerodynamic
1024 micrometeorological gradient method, *Journal of Geophysical Research: Atmospheres*,
1025 110, 2005.

1026 Ferek, R. J., Reid, J. S., Hobbs, P. V., Blake, D. R., and Lioussé, C.: Emission factors
1027 of hydrocarbons, halocarbons, trace gases and particles from biomass burning in Brazil,
1028 *Journal of Geophysical Research*, 103, 107-132, 1998.

1029 Giglio, L., Randerson, J. T., and Werf, G. R.: Analysis of daily, monthly, and annual
1030 burned area using the fourth-generation global fire emissions database (GFED4),
1031 *Journal of Geophysical Research: Biogeosciences*, 118, 317-328, 2013.

1032 Govender, N., Trollope, W. S., and Van Wilgen, B. W.: The effect of fire season, fire
1033 frequency, rainfall and management on fire intensity in savanna vegetation in South
1034 Africa, *Journal of Applied Ecology*, 43, 748-758, 2006.

1035 Griffith, D. W. T.: Synthetic calibration and quantitative analysis of gas-phase FT-IR
1036 spectra, *Applied Spectroscopy*, 50, 59-70, 1996.

1037 Griffith, D. W. T., Deutscher, N. M., Caldow, C., Kettlewell, G., Riggenbach, M., and
1038 Hammer, S.: A Fourier transform infrared trace gas and isotope analyser for
1039 atmospheric applications, *Atmos. Meas. Tech.*, 5, 2481-2498, 2012.

1040 Guieu, C., Bonnet, S., Wagener, T., and Loÿe-Pilot, M. D.: Biomass burning as a source
1041 of dissolved iron to the open ocean?, *Geophysical Research Letters*, 32, 2005.

1042 Gustin, M. S., Lindberg, S. E., and Weisberg, P. J.: An update on the natural sources
1043 and sinks of atmospheric mercury, *Applied Geochemistry*, 23, 482-493, 2008.

1044 Honninger, G., von Friedeburg, C., and Platt, U.: Multi axis differential optical
1045 absorption spectroscopy (MAX-DOAS), *Atmospheric Chemistry and Physics*, 4, 231-
1046 254, 2004.

1047 Howard, D., Nelson, P. F., Edwards, G. C., Morrison, A. L., Fisher, J. A., Ward, J.,
1048 Harnwell, J., van der Schoot, M., Atkinson, B., Chambers, S. D., Griffiths, A. D.,
1049 Werczynski, S., and Williams, A. G.: Atmospheric mercury in the southern hemisphere
1050 tropics: seasonal and diurnal variations and influence of inter-hemispheric transport,
1051 *Atmos. Chem. Phys. Discuss.*, 2017, 1-20, 10.5194/acp-2017-307, 2017.

1052 Iinuma, Y., Engling, G., Puxbaum, H., and Herrmann, H.: A highly resolved anion-
1053 exchange chromatographic method for determination of saccharidic tracers for biomass

1054 combustion and primary bio-particles in atmospheric aerosol, *Atmospheric*
 1055 *Environment*, 43, 1367-1371, 2009.
 1056 Ito, A.: Mega fire emissions in Siberia: potential supply of bioavailable iron from
 1057 forests to the ocean, *Biogeosciences*, 8, 1679-1697, 2011.
 1058 Jacobson, M. Z.: Strong radiative heating due to the mixing state of black carbon in
 1059 atmospheric aerosols, *Nature*, 409, 695-697, 2001.
 1060 Kaiser, J. W., and Keywood, M.: Preface for *Atmos. Env. Special issue on IBBI*,
 1061 *Atmospheric Environment*, 121, 1-3, 2015.
 1062 Keil, A., and Haywood, J. M.: Solar radiative forcing by biomass burning aerosol
 1063 particles during SAFARI 2000: A case study based on measured aerosol and cloud
 1064 properties, *Journal of Geophysical Research: Atmospheres*, 108, 2003.
 1065 Keywood, M., Kanakidou, M., Stohl, A., Dentener, F., Grassi, G., Meyer, C. P.,
 1066 Torseth, K., Edwards, D., Thompson, A. M., Lohmann, U., and Burrows, J.: Fire in the
 1067 air: Biomass burning impacts in a changing climate, *Critical Reviews in Environmental*
 1068 *Science and Technology*, 43, 40-83, 2013.
 1069 Landis, M. S., Stevens, R. K., Schaedlich, F., and Prestbo, E. M.: Development and
 1070 characterization of an annular denuder methodology for the measurement of divalent
 1071 inorganic reactive gaseous mercury in ambient air, *Environmental science &*
 1072 *technology*, 36, 3000-3009, 2002.
 1073 LaRoche, J., and Breitbarth, E.: Importance of the diazotrophs as a source of new
 1074 nitrogen in the ocean, *Journal of Sea Research*, 53, 67-91, 2005.
 1075 Lawson, S. J., Keywood, M. D., Galbally, I. E., Gras, J. L., Caine, J. M., Cope, M. E.,
 1076 Krummel, P. B., Fraser, P. J., Steele, L. P., Bentley, S. T., Meyer, C. P., Ristovski, Z.,
 1077 and Goldstein, A. H.: Biomass burning emissions of trace gases and particles in marine
 1078 air at Cape Grim, Tasmania, *Atmospheric Chemistry and Physics*, 15, 13393-13411,
 1079 2015.
 1080 Lin, N.-H., Tsay, S.-C., Maring, H. B., Yen, M.-C., Sheu, G.-R., Wang, S.-H., Chi, K.
 1081 H., Chuang, M.-T., Ou-Yang, C.-F., and Fu, J. S.: An overview of regional experiments
 1082 on biomass burning aerosols and related pollutants in Southeast Asia: From BASE-
 1083 ASIA and the Dongsha Experiment to 7-SEAS, *Atmospheric Environment*, 78, 1-19,
 1084 2013.
 1085 Lioussé, C., Devaux, C., Dulac, F., and Cachier, H.: Aging of savanna biomass burning
 1086 aerosols: Consequences on their optical properties, *Journal of Atmospheric Chemistry*,
 1087 22, 1-17, 1995.
 1088 Manninen, H. E., Petaja, T., Asmi, E., Riipinen, I., Nieminen, T., Mikkilä, J., Horrak,
 1089 U., Mirme, A., Mirme, S., Laakso, L., Kerminen, V. M., and Kulmala, M.: Long-term
 1090 field measurements of charged and neutral clusters using Neutral cluster and Air Ion
 1091 Spectrometer (NAIS), *Boreal Environment Research*, 14, 591-605, 2009.
 1092 Meyer, C., Cook, G., Reisen, F., Smith, T., Tattaris, M., Russell-Smith, J., Maier, S.,
 1093 Yates, C., and Wooster, M.: Direct measurements of the seasonality of emission factors
 1094 from savanna fires in northern Australia, *Journal of Geophysical Research:*
 1095 *Atmospheres (1984–2012)*, 117, 2012.
 1096 Meyer, C. P., Luhar, A. K., and Mitchell, R. M.: Biomass burning emissions over
 1097 northern Australia constrained by aerosol measurements: I—Modelling the distribution
 1098 of hourly emissions, *Atmospheric Environment*, 42, 1629-1646, 2008.
 1099 Mirme, A., Tamm, E., Mordas, G., Vana, M., Uin, J., Mirme, S., Bernotas, T., Laakso,
 1100 L., Hirsikko, A., and Kulmala, M.: A wide-range multi-channel Air Ion Spectrometer,
 1101 *Boreal Environmental Research*, 12, 247-264, 2007.
 1102 National-Environment-Protection-Council-Service-Corporation: National
 1103 Environment Protection (Air Toxics) Measure, 2011.

1104 Paris, R., Desboeufs, K., Formenti, P., Nava, S., and Chou, C.: Chemical
 1105 characterisation of iron in dust and biomass burning aerosols during AMMA-
 1106 SOP0/DABEX: implication for iron solubility, *Atmospheric Chemistry and Physics*,
 1107 10, 4273-4282, 2010.
 1108 Penner, J., Chuang, C., and Grant, K.: Climate forcing by carbonaceous and sulfate
 1109 aerosols, *Climate Dynamics*, 14, 839-851, 1998.
 1110 Rea, A. W., Lindberg, S. E., Scherbatskoy, T., and Keeler, G. J.: Mercury accumulation
 1111 in foliage over time in two northern mixed-hardwood forests, *Water, Air, and Soil*
 1112 *Pollution*, 133(1-4), 49-67, 2002.
 1113 Russell-Smith, J., Yates, C. P., Whitehead, P. J., Smith, R., Craig, R., Allan, G. E.,
 1114 Thackway, R., Frakes, I., Cridland, S., Meyer, M. C. P., and Gill, M.: Bushfires' down
 1115 under': patterns and implications of contemporary Australian landscape burning,
 1116 *International Journal of Wildland Fire*, 16, 361-377, 2007.
 1117 Russell-Smith, J., Cook, G. D., Cooke, P. M., Edwards, A. C., Lendrum, M., Meyer,
 1118 C., and Whitehead, P. J.: Managing fire regimes in north Australian savannas: applying
 1119 Aboriginal approaches to contemporary global problems, *Frontiers in Ecology and the*
 1120 *Environment*, 11, e55-e63, 2013.
 1121 Saarikoski, S., Sillanpää, M., Sofiev, M., Timonen, H., Saarnio, K., Teinilä, K.,
 1122 Karppinen, A., Kukkonen, J., and Hillamo, R.: Chemical composition of aerosols
 1123 during a major biomass burning episode over northern Europe in spring 2006:
 1124 Experimental and modelling assessments, *Atmospheric Environment*, 41, 3577-3589,
 1125 2007.
 1126 Sedwick, P. N., Sholkovitz, E. R., and Church, T. M.: Impact of anthropogenic
 1127 combustion emissions on the fractional solubility of aerosol iron: Evidence from the
 1128 Sargasso Sea, *Geochemistry, Geophysics, Geosystems*, 8, 2007.
 1129 Shi, Y., Matsunaga, T., Saito, M., Yamaguchi, Y., and Chen, X.: Comparison of global
 1130 inventories of CO₂ emissions from biomass burning during 2002–2011 derived from
 1131 multiple satellite products, *Environmental Pollution*, 206, 479-487, 2015.
 1132 Singh, H., Brune, W., Crawford, J., Jacob, D. J., and Russell, P.: Overview of the
 1133 summer 2004 Intercontinental Chemical Transport Experiment–North America
 1134 (INTEX-A), *Journal of Geophysical Research: Atmospheres*, 111, 2006.
 1135 Sinreich, R., Friess, U., Wagner, T., and Platt, U.: Multi axis differential optical
 1136 absorption spectroscopy (MAX-DOAS) of gas and aerosol distributions, *Faraday*
 1137 *Discuss*, 130, 153-164, 2005.
 1138 Sprovieri, F., Pirrone, N., Bencardino, M., D'Amore, F., Carbone, F., Cinnirella, S.,
 1139 Mannarino, V., Landis, M., Ebinghaus, R., Weigelt, A., Brunke, E. G., Labuschagne,
 1140 C., Martin, L., Munthe, J., Wängberg, I., Artaxo, P., Morais, F., Cairns, W., Barbante,
 1141 C., Diéguez, M. D. C., Garcia, P. E., Dommergue, A., Angot, H., Magand, O., Skov,
 1142 H., Horvat, M., Kotnik, J., Read, K. A., Neves, L. M., Gawlik, B. M., Sena, F.,
 1143 Mashyanov, N., Obolkin, V. A., Wip, D., Feng, X. B., Zhang, H., Fu, X.,
 1144 Ramachandran, R., Cossa, D., Knoery, J., Maruszak, N., Nerentorp, M., and Norstrom,
 1145 C.: Atmospheric Mercury Concentrations observed at ground-based monitoring sites
 1146 globally distributed in the framework of the GMOS network, *Atmospheric Chemistry*
 1147 *and Physics Discussions*, 2016, 1-32, 2016.
 1148 Steffen, A., Douglas, T., Amyot, M., Ariya, P., Aspö, K., Berg, T., Bottenheim, J.,
 1149 Brooks, S., Cobbett, F., Dastoor, A., Dommergue, A., Ebinghaus, R., Ferrari, C.,
 1150 Gardfeldt, K., Goodsite, M. E., Lean, D., Poulain, A. J., Scherz, C., Skov, H., Sommar,
 1151 J., and Temme, C.: A synthesis of atmospheric mercury depletion event chemistry in
 1152 the atmosphere and snow, *Atmospheric Chemistry and Physics*, 8, 1445-1482, 2008.

1153 Stockwell, C., Yokelson, R., Kreidenweis, S., Robinson, A., DeMott, P., Sullivan, R.,
1154 Reardon, J., Ryan, K., Griffith, D., and Stevens, L.: Trace gas emissions from
1155 combustion of peat, crop residue, domestic biofuels, grasses, and other fuels:
1156 configuration and Fourier transform infrared (FTIR) component of the fourth Fire Lab
1157 at Missoula Experiment (FLAME-4), *Atmospheric Chemistry and Physics*, 9727, 2014.
1158 Tuch, T. M., Haudek, A., Müller, T., Nowak, A., Wex, H., and Wiedensohler, A.:
1159 Design and performance of an automatic regenerating adsorption aerosol dryer for
1160 continuous operation at monitoring sites, *Atmos. Meas. Tech.*, 2, 417-422, 2009.
1161 van der Werf, G. R., Randerson, J. T., Giglio, L., Collatz, G., Mu, M., Kasibhatla, P.
1162 S., Morton, D. C., DeFries, R., Jin, Y. v., and van Leeuwen, T. T.: Global fire emissions
1163 and the contribution of deforestation, savanna, forest, agricultural, and peat fires (1997–
1164 2009), *Atmospheric Chemistry and Physics*, 10, 11707-11735, 2010.
1165 Wang, X., Thai, P. K., Mallet, M., Desservettaz, M., Hawker, D. W., Keywood, M.,
1166 Miljevic, B., Paton-Walsh, C., Gallen, M., and Mueller, J. F.: Emissions of selected
1167 semivolatile organic chemicals from forest and savannah fires, *Environmental science
& technology*, 51, 1293-1302, 2017.
1169 Whittlestone, S., and Zahorowski, W.: Baseline radon detectors for shipboard use:
1170 Development and deployment in the First Aerosol Characterization Experiment (ACE
1171 1), *Journal of Geophysical Research: Atmospheres*, 103, 16743-16751, 1998.
1172 Winton, V., Bowie, A., Edwards, R., Keywood, M., Townsend, A., van der Merwe, P.,
1173 and Bollhöfer, A.: Fractional iron solubility of atmospheric iron inputs to the Southern
1174 Ocean, *Marine Chemistry*, 177, 20-32, 2015.
1175 Winton, V., Edwards, R., Bowie, A., Keywood, M., Williams, A., Chambers, S.,
1176 Selleck, P., Desservettaz, M., Mallet, M., and Paton-Walsh, C.: Dry season aerosol iron
1177 solubility in tropical northern Australia, *Atmospheric Chemistry and Physics
Discussions*, doi:10.5194/acp-2016-419, 2016.
1179 Wong, J., and Li, Z.: Retrieval of optical depth for heavy smoke aerosol plumes:
1180 uncertainties and sensitivities to the optical properties, *Journal of the Atmospheric
Sciences*, 59, 250-261, 2002.
1182 Yokelson, R. J., Crounse, J. D., DeCarlo, P. F., Karl, T., Urbanski, S., Atlas, E.,
1183 Campos, T., Shinozuka, Y., Kapustin, V., Clarke, A. D., Weinheimer, A., Knapp, D. J.,
1184 Montzka, D. D., Holloway, J., Weibring, P., Flocke, F., Zheng, W., Toohey, D.,
1185 Wennberg, P. O., Wiedinmyer, C., Mauldin, L., Fried, A., Richter, D., Walega, J.,
1186 Jimenez, J. L., Adachi, K., Buseck, P. R., Hall, S. R., and Shetter, R.: Emissions from
1187 biomass burning in the Yucatan, *Atmospheric Chemistry and Physics*, 9, 5785-5812,
1188 2009.

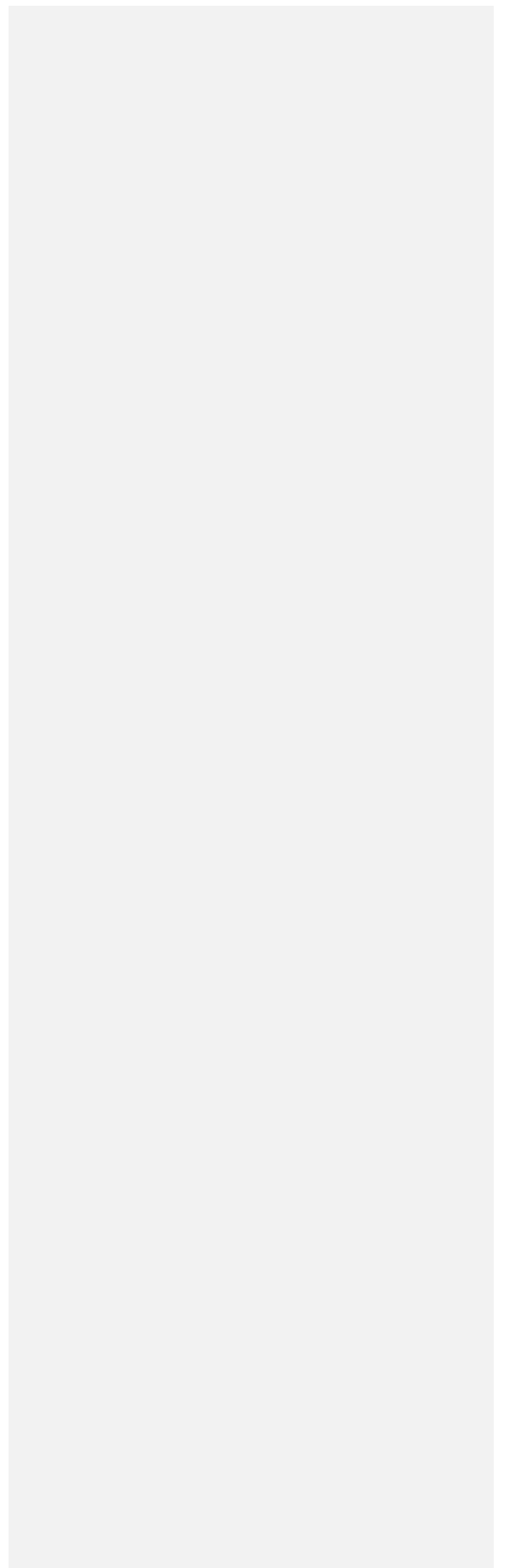
1189

1190

Formatted: Justified, Line spacing: double

Formatted: Font color: Text 1

Formatted: Heading 1



Page 9: [1] Formatted **Marc Mallet** **5/15/17 12:52:00 AM**

Centered, Position:Horizontal: Left, Relative to: Column, Vertical: 0", Relative to: Paragraph,
Horizontal: 0.13", Wrap Around

Page 9: [2] Formatted **Marc Mallet** **5/15/17 12:52:00 AM**

Centered, Position:Horizontal: Left, Relative to: Column, Vertical: 0", Relative to: Paragraph,
Horizontal: 0.13", Wrap Around

Page 9: [3] Formatted **Marc Mallet** **5/15/17 12:52:00 AM**

Centered, Position:Horizontal: Left, Relative to: Column, Vertical: 0", Relative to: Paragraph,
Horizontal: 0.13", Wrap Around

Page 9: [4] Formatted **Marc Mallet** **5/15/17 12:52:00 AM**

Centered, Position:Horizontal: Left, Relative to: Column, Vertical: 0", Relative to: Paragraph,
Horizontal: 0.13", Wrap Around

Page 9: [5] Formatted **Marc Mallet** **5/15/17 12:52:00 AM**

Centered, Position:Horizontal: Left, Relative to: Column, Vertical: 0", Relative to: Paragraph,
Horizontal: 0.13", Wrap Around

Page 14: [6] Deleted **Marc Mallet** **5/1/17 10:12:00 PM**

Radon-222 (radon) is a naturally occurring radioactive noble gas that arises from the alpha-particle decay of radium-226, which is ubiquitous in most soil and rock types. With a half-life of 3.82 days, radon has thus proven to be an excellent indicator of recent (within 2-3 weeks) terrestrial influences on air masses for observations at coastal or island sites (Chambers et al., 2014). Radon is unreactive and poorly soluble, and its only atmospheric sink is radioactive decay. Furthermore, it has a half-life comparable to the lifetimes of short-lived atmospheric pollutants (e.g., NO_x, SO₂) and atmospheric residence time of water and

aerosols. Radon's unique combination of physical characteristics make it an ideal tracer for (i) regional air mass transport studies, in which it is often used in conjunction with air mass back trajectories for fetch analyses (Williams et al., 2009; Chambers et al., 2014); (ii) investigations of vertical mixing processes within the daytime convective boundary layer (Williams et al., 2011) or nocturnal boundary layer (Chambers et al., 2015); (iii) identifying periods of minimal terrestrial influence on a measured air mass ("baseline" studies; (Chambers et al., 2016)); (iv) performing regional flux or inventory analyses for trace atmospheric species with similar source distributions (Biraud et al., 2000) and (v) evaluating the performance of transport and mixing schemes in climate and chemical-transport models (Locatelli et al., 2015).

Page 24: [7] Deleted

Marc Mallet

5/2/17 1:32:00 AM

Afternoon radon concentrations provide further information regarding the regional air mass fetch and the degree of contact with the land surface (red line, Figure 3a). Over the campaign period, air masses with the least terrestrial fetch (low radon indicates strongest oceanic signature) were observed on June 4-6 and 20-22, whereas June 8-9, 17-18 and 29-30 represented periods of particularly extensive continental fetch.

Page 26: [8] Deleted

Marc Mallet

5/2/17 1:31:00 AM

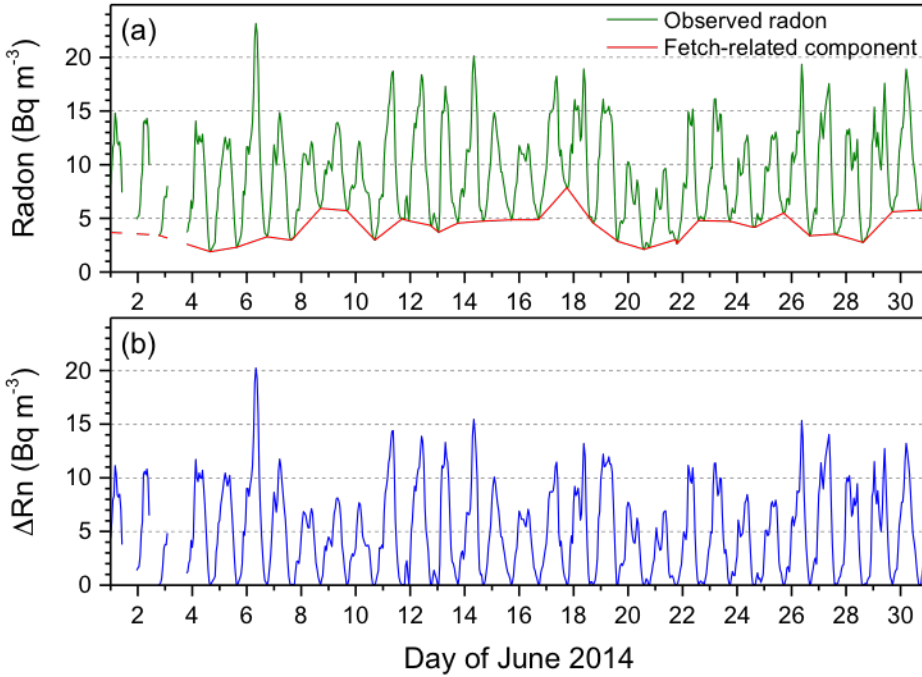


Figure 3 Hourly ATARS radon observations for June 2014: (a) observed hourly data, and afternoon-to-afternoon interpolated values (indicative of changes in the regional air mass fetch); and (b) difference in radon concentration between the hourly observations and interpolated afternoon values (indicative of diurnal variability).

A pronounced diurnal variability can clearly be seen in the ΔRn signal (Figure 3b). Mean hourly diurnal composites of radon concentrations, wind speed, wind direction and dew point temperature at the ATARS site during the period of the SAFIRED campaign are shown in Figure 4. Following the technique described in Chambers et al. (2016), these composites have been computed separately for three diurnal mixing categories based on the mean ΔRn over the 12 hour period 2000-0800 h:

Strong mixing: $\Delta Rn_{12} < 5400 \text{ mBq m}^{-3}$

Moderate mixing: $5400 \leq \Delta Rn_{12} < 6700 \text{ mBq m}^{-3}$

Weak mixing: $\Delta Rn_{12} \geq 6700 \text{ mBq m}^{-3}$

The air masses predominantly originated from the southeast as indicated in Figure 1 and Figure 4c. Starting from approximately 10:00 am each morning, however, sea breeze circulations slowly turn the measured wind direction around from southeast to northeast, before reverting back to the

dominant wind direction again at around midnight. Wind speeds reached a maximum just before midday and were at their lowest just before midnight (Figure 4b). The “strong mixing” category was associated with generally higher wind speeds, which cause increased mechanical turbulence leading to deeper nocturnal mixing layers (i.e., hinder the development of a shallow nocturnal inversion layer).

Gas and Aerosol measurements

The campaign average, standard deviation, median and Q25/Q75 values for the major gaseous and aerosol species are shown in Table 1. The median values for each species are likely to be representative of background concentrations in this region. The average concentrations for most species were higher than the median concentrations, due to the periods of close or intense fires.

The extent of the influence of these close fires are demonstrated by the maximum concentrations.

Table 1 The campaign average, standard deviation, maximum, median, Q25 and Q75 values for key measured gas and aerosol species. All parts-per notation refer to mole fractions unless otherwise indicated.

Species (unit)	Average	Standard deviation	Maximum	Median	Q25	Q75
CO (ppb)	229	494	18900	130	87	214
CO ₂ (ppm)	404.68	11.539	513.578	402.454	394.728	411.299
O ₃ (ppbv)	24.616	9.903	99.784	22.771	17.896	29.778
CH ₄ (ppb)	1839.88	68.06	3766.81	1820.11	1802.26	1852.97
N ₂ O (ppb)	326.329	0.449	334.871	326.276	326.121	326.444
GEM (ng m ⁻³)	0.992	0.081	1.734	0.986	0.952	1.020
Acetonitrile (ppb)	0.351	0.629	9.775	0.197	0.129	0.337

Organics (ug m⁻³)	11.081	22.385	347.657	4.160	2.335	13.279
SO₄²⁻ (ug m⁻³)	0.514	0.318	2.254	0.411	0.294	0.679
NH₄⁺ (ug m⁻³)	0.351	0.676	18.17	0.180	0.096	0.415
NO₃⁻ (ug m⁻³)	0.187	0.456	10.925	0.042	0.004	0.189
Cl⁻ (ug m⁻³)	0.166	1.271	53.270	0.029	0.016	0.076
PNC (cm⁻³)	8182	19031	40300	2032	2032	8335
Mode diameter (nm)	104	31	-	102	85	122
Geom. SD	1.71	0.13	-	1.70	1.65	1.75

In order to demonstrate the influence of close fires and the changing inversion layer, the time series of major greenhouse gases (CO, CO₂, CH₄ and N₂O), gaseous elemental mercury, acetonitrile and ozone throughout the campaign are shown in Figure 5. Sub-micron non-refractory aerosol organic, sulfate, ammonium and nitrate mass concentrations, organic mass fraction, PM₁ OC and EC mass concentrations and particle size distributions for the sampling period are shown in Figure 6. Periods of missing data correspond to times when instruments were not operating. Most of these time series display a clear diurnal trend as a result of the varying inversion layer height. Other enhancements in concentrations can be clearly seen and correspond to periods of frequent close fires (Figure 2). Over the entire sampling period from the 29th of May 2014 until the 28th of June 2014, four biomass burning related periods (BBP) and a "coastal" period (CP) have been distinguished. The dates for these periods are shown in Table 2. These periods are also displayed in Figure 5 and Figure 6.

Table 2 The start and end dates for the four identified Biomass Burning Periods (BBP1, BBP2, BBP3 and BBP4) and the Coastal Period (CP).

Period	Start date (mm/dd/yy hh:mm)	End date (mm/dd/yy hh:mm)
BBP1	05/30/14 00:00	05/31/14 23:59
BBP2	06/06/14 00:00	06/12/14 23:59
BBP3	06/14/14 00:00	06/17/14 23:59
CP	06/19/14 12:00	06/22/14 23:59
BBP3	06/23/14 00:00	06/28/14 23:59

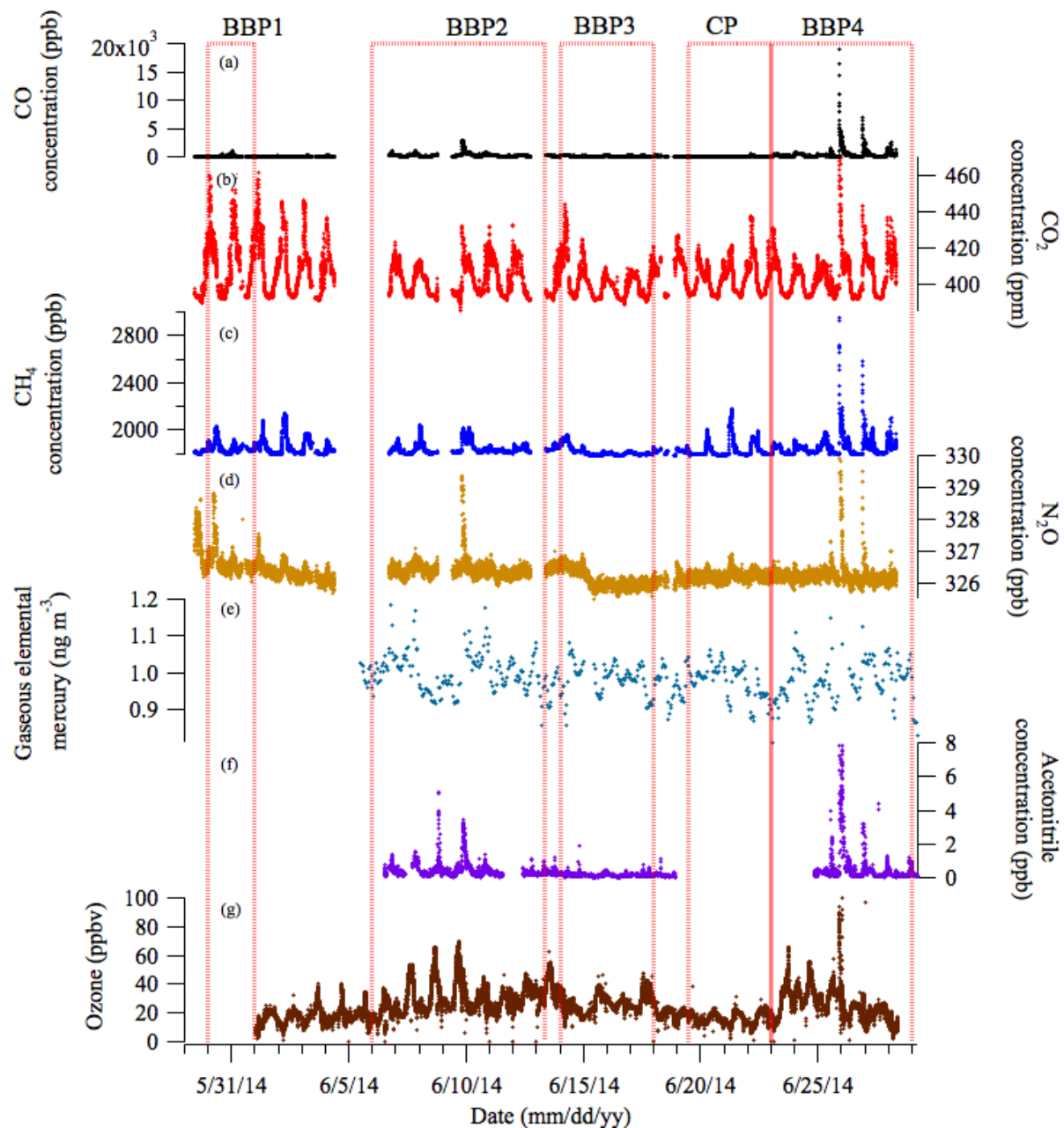


Figure 5 The time series of the major measured gaseous species during the SAFIRED campaign: (a) carbon monoxide, (b) carbon dioxide, (c) methane, (d) nitrogen dioxide, (e) gaseous elemental mercury, (f) acetonitrile and (g) ozone and $\Delta O_3/\Delta CO$. The biomass burning and coastal periods are indicated by the red dotted lines. All parts-per notation refer to mole fractions unless otherwise indicated.

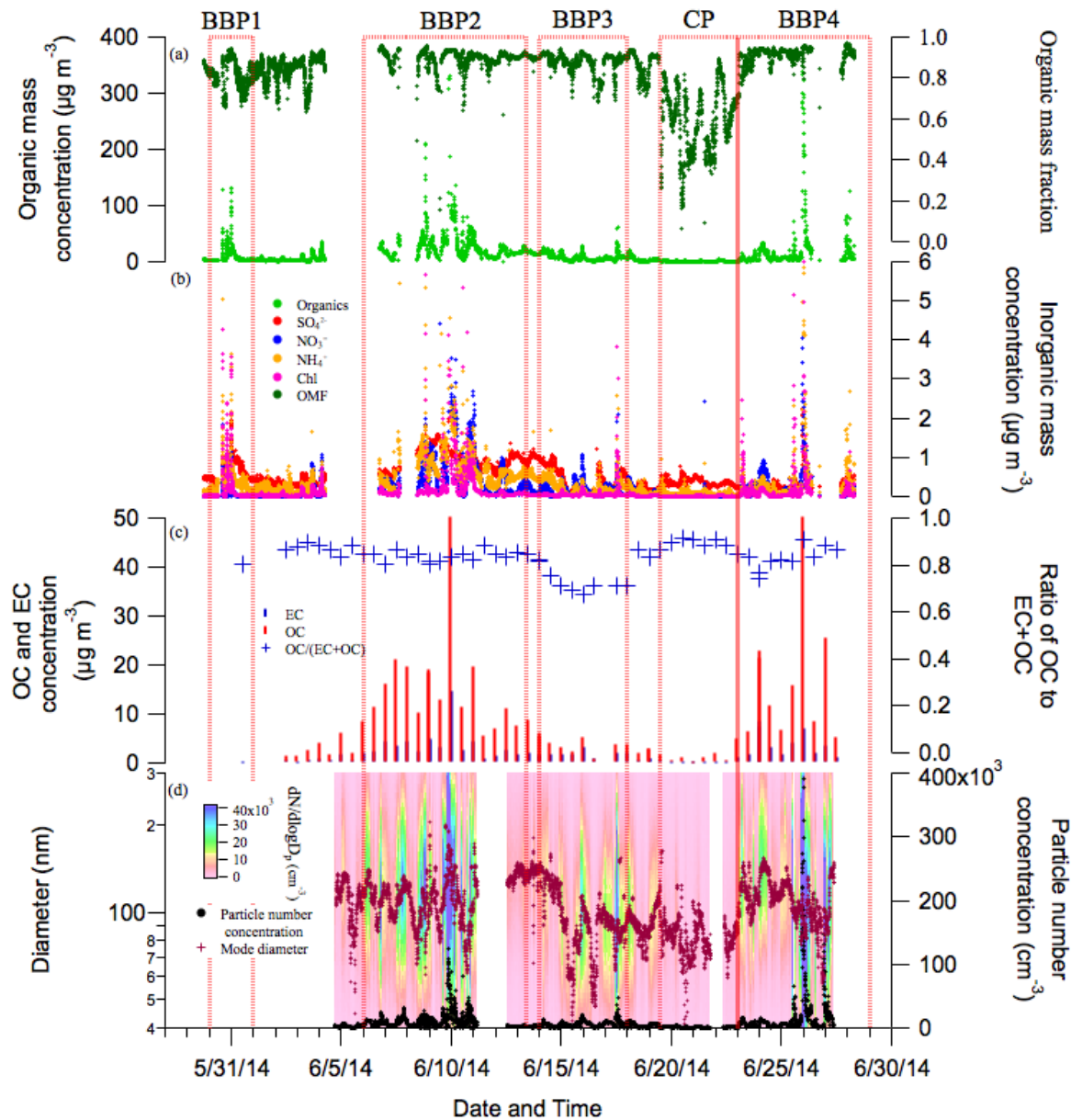


Figure 6 The times series of the major aerosol properties during the SAFIRED campaign: (a) the non-refractory PM_{10} organic mass concentration (left) and organic mass fraction (right), (b) the inorganic non-refractory PM_{10} mass concentrations, (c) the 12-hour filter OC and EC PM_{10} mass concentrations (left) and the ratio of OC to OC+EC (right), (d) the particle size distributions and particle size mode (left) and the total particle number concentration (right) and (e) the wind direction at ATARS.

Over the campaign organics dominated the non-refractory sub-micron aerosol mass contributing, on average 90% (median; 86%) of the total mass. Sulphate, nitrates, ammonium and chloride species contributed the rest of this mass, with the largest contributions from sulphate and ammonium. Sulphate contributions were very significant during the coastal period, contributing

up to 32% of the total mass. Although chlorides contributed the least to the total mass, on average, during clear biomass burning events where sharp increases in CO and organics were observed, chlorides made up the largest component of inorganic aerosol. The maximum chloride concentration during the campaign reached $53 \mu\text{g m}^{-3}$. High soil and vegetation chloride contents have been observed in savannah and coastal environments (Lobert et al., 1999; Andreae et al., 1996). The strong elevations of chloride signals observed, particularly during burning events BBP1, BBP2 and BBP4 are likely a result of emission of these chloride ions. Outside of the "burning events" where very sharp increases in concentrations were observed, chloride concentrations were very low. This either suggests that these chloride species are short-lived, or only present in fires very close to the coast and therefore the ATARS site.

Page 31: [10] Formatted **Marc Mallet** **11/8/16 11:22:00 PM**

Font:Not Bold, Font color: Text 1

Page 31: [10] Formatted **Marc Mallet** **11/8/16 11:22:00 PM**

Font:Not Bold, Font color: Text 1

Page 31: [10] Formatted **Marc Mallet** **11/8/16 11:22:00 PM**

Font:Not Bold, Font color: Text 1

Page 31: [10] Formatted **Marc Mallet** **11/8/16 11:22:00 PM**

Font:Not Bold, Font color: Text 1

Page 31: [10] Formatted **Marc Mallet** **11/8/16 11:22:00 PM**

Font:Not Bold, Font color: Text 1

Page 31: [11] Formatted **Marc Mallet** **11/8/16 11:22:00 PM**

Font:10 pt, Font color: Text 1

Page 31: [11] Formatted **Marc Mallet** **11/8/16 11:22:00 PM**

Font:10 pt, Font color: Text 1

Page 31: [11] Formatted **Marc Mallet** **11/8/16 11:22:00 PM**

Font:10 pt, Font color: Text 1

Page 31: [11] Formatted **Marc Mallet** **11/8/16 11:22:00 PM**

Font:10 pt, Font color: Text 1

Page 31: [11] Formatted **Marc Mallet** **11/8/16 11:22:00 PM**

Font:10 pt, Font color: Text 1

Page 31: [11] Formatted **Marc Mallet** **11/8/16 11:22:00 PM**

Font:10 pt, Font color: Text 1

Page 31: [11] Formatted **Marc Mallet** **11/8/16 11:22:00 PM**

Font:10 pt, Font color: Text 1

Page 31: [11] Formatted **Marc Mallet** **11/8/16 11:22:00 PM**

Font:10 pt, Font color: Text 1

Page 31: [11] Formatted **Marc Mallet** **11/8/16 11:22:00 PM**

Font:10 pt, Font color: Text 1

Page 31: [11] Formatted **Marc Mallet** **11/8/16 11:22:00 PM**

Font:10 pt, Font color: Text 1

Page 31: [11] Formatted **Marc Mallet** **11/8/16 11:22:00 PM**

Font:10 pt, Font color: Text 1

Page 31: [11] Formatted **Marc Mallet** **11/8/16 11:22:00 PM**

Font:10 pt, Font color: Text 1

Page 31: [11] Formatted **Marc Mallet** **11/8/16 11:22:00 PM**

Font:10 pt, Font color: Text 1

Page 31: [11] Formatted **Marc Mallet** **11/8/16 11:22:00 PM**

Font:10 pt, Font color: Text 1

Page 31: [11] Formatted	Marc Mallet	11/8/16 11:22:00 PM
--------------------------------	--------------------	----------------------------

Font:10 pt, Font color: Text 1

Page 31: [11] Formatted	Marc Mallet	11/8/16 11:22:00 PM
--------------------------------	--------------------	----------------------------

Font:10 pt, Font color: Text 1

Page 31: [11] Formatted	Marc Mallet	11/8/16 11:22:00 PM
--------------------------------	--------------------	----------------------------

Font:10 pt, Font color: Text 1

Page 31: [11] Formatted	Marc Mallet	11/8/16 11:22:00 PM
--------------------------------	--------------------	----------------------------

Font:10 pt, Font color: Text 1

Page 31: [11] Formatted	Marc Mallet	11/8/16 11:22:00 PM
--------------------------------	--------------------	----------------------------

Font:10 pt, Font color: Text 1

Page 31: [11] Formatted	Marc Mallet	11/8/16 11:22:00 PM
--------------------------------	--------------------	----------------------------

Font:10 pt, Font color: Text 1

Page 31: [11] Formatted	Marc Mallet	11/8/16 11:22:00 PM
--------------------------------	--------------------	----------------------------

Font:10 pt, Font color: Text 1

Page 31: [11] Formatted	Marc Mallet	11/8/16 11:22:00 PM
--------------------------------	--------------------	----------------------------

Font:10 pt, Font color: Text 1

Page 31: [11] Formatted	Marc Mallet	11/8/16 11:22:00 PM
--------------------------------	--------------------	----------------------------

Font:10 pt, Font color: Text 1

Page 31: [11] Formatted	Marc Mallet	11/8/16 11:22:00 PM
--------------------------------	--------------------	----------------------------

Font:10 pt, Font color: Text 1

Page 31: [11] Formatted	Marc Mallet	11/8/16 11:22:00 PM
--------------------------------	--------------------	----------------------------

Font:10 pt, Font color: Text 1

Page 31: [11] Formatted	Marc Mallet	11/8/16 11:22:00 PM
--------------------------------	--------------------	----------------------------

Font:10 pt, Font color: Text 1

Page 31: [11] Formatted **Marc Mallet** **11/8/16 11:22:00 PM**

Font:10 pt, Font color: Text 1

Page 31: [11] Formatted **Marc Mallet** **11/8/16 11:22:00 PM**

Font:10 pt, Font color: Text 1

Page 31: [11] Formatted **Marc Mallet** **11/8/16 11:22:00 PM**

Font:10 pt, Font color: Text 1

Page 31: [11] Formatted **Marc Mallet** **11/8/16 11:22:00 PM**

Font:10 pt, Font color: Text 1

Page 31: [11] Formatted **Marc Mallet** **11/8/16 11:22:00 PM**

Font:10 pt, Font color: Text 1

Page 31: [11] Formatted **Marc Mallet** **11/8/16 11:22:00 PM**

Font:10 pt, Font color: Text 1

Page 31: [11] Formatted **Marc Mallet** **11/8/16 11:22:00 PM**

Font:10 pt, Font color: Text 1

Page 31: [11] Formatted **Marc Mallet** **11/8/16 11:22:00 PM**

Font:10 pt, Font color: Text 1

Page 31: [11] Formatted **Marc Mallet** **11/8/16 11:22:00 PM**

Font:10 pt, Font color: Text 1

Page 31: [11] Formatted **Marc Mallet** **11/8/16 11:22:00 PM**

Font:10 pt, Font color: Text 1

Page 31: [11] Formatted **Marc Mallet** **11/8/16 11:22:00 PM**

Font:10 pt, Font color: Text 1

Page 31: [11] Formatted **Marc Mallet** **11/8/16 11:22:00 PM**

Font:10 pt, Font color: Text 1

Page 31: [11] Formatted **Marc Mallet** **11/8/16 11:22:00 PM**

Font:10 pt, Font color: Text 1

Page 31: [11] Formatted **Marc Mallet** **11/8/16 11:22:00 PM**

Font:10 pt, Font color: Text 1

Page 31: [11] Formatted **Marc Mallet** **11/8/16 11:22:00 PM**

Font:10 pt, Font color: Text 1

Page 31: [11] Formatted **Marc Mallet** **11/8/16 11:22:00 PM**

Font:10 pt, Font color: Text 1

Page 31: [11] Formatted **Marc Mallet** **11/8/16 11:22:00 PM**

Font:10 pt, Font color: Text 1

Page 31: [11] Formatted **Marc Mallet** **11/8/16 11:22:00 PM**

Font:10 pt, Font color: Text 1

Page 31: [11] Formatted **Marc Mallet** **11/8/16 11:22:00 PM**

Font:10 pt, Font color: Text 1

Page 31: [11] Formatted **Marc Mallet** **11/8/16 11:22:00 PM**

Font:10 pt, Font color: Text 1

Page 31: [11] Formatted **Marc Mallet** **11/8/16 11:22:00 PM**

Font:10 pt, Font color: Text 1

Page 31: [11] Formatted **Marc Mallet** **11/8/16 11:22:00 PM**

Font:10 pt, Font color: Text 1

Page 31: [11] Formatted **Marc Mallet** **11/8/16 11:22:00 PM**

Font:10 pt, Font color: Text 1

Page 31: [11] Formatted **Marc Mallet** **11/8/16 11:22:00 PM**

Font:10 pt, Font color: Text 1

Page 31: [11] Formatted **Marc Mallet** **11/8/16 11:22:00 PM**

Font:10 pt, Font color: Text 1

Page 31: [11] Formatted **Marc Mallet** **11/8/16 11:22:00 PM**

Font:10 pt, Font color: Text 1

Page 31: [11] Formatted **Marc Mallet** **11/8/16 11:22:00 PM**

Font:10 pt, Font color: Text 1

Page 31: [11] Formatted **Marc Mallet** **11/8/16 11:22:00 PM**

Font:10 pt, Font color: Text 1

Page 31: [11] Formatted **Marc Mallet** **11/8/16 11:22:00 PM**

Font:10 pt, Font color: Text 1

Page 31: [11] Formatted **Marc Mallet** **11/8/16 11:22:00 PM**

Font:10 pt, Font color: Text 1

Page 31: [11] Formatted **Marc Mallet** **11/8/16 11:22:00 PM**

Font:10 pt, Font color: Text 1

Page 31: [11] Formatted **Marc Mallet** **11/8/16 11:22:00 PM**

Font:10 pt, Font color: Text 1

Page 31: [11] Formatted **Marc Mallet** **11/8/16 11:22:00 PM**

Font:10 pt, Font color: Text 1

Page 31: [11] Formatted **Marc Mallet** **11/8/16 11:22:00 PM**

Font:10 pt, Font color: Text 1

Page 31: [11] Formatted **Marc Mallet** **11/8/16 11:22:00 PM**

Font:10 pt, Font color: Text 1

Page 31: [11] Formatted **Marc Mallet** **11/8/16 11:22:00 PM**

Font:10 pt, Font color: Text 1

Page 31: [11] Formatted **Marc Mallet** **11/8/16 11:22:00 PM**

Font:10 pt, Font color: Text 1

Page 31: [11] Formatted **Marc Mallet** **11/8/16 11:22:00 PM**

Font:10 pt, Font color: Text 1

Page 31: [11] Formatted **Marc Mallet** **11/8/16 11:22:00 PM**

Font:10 pt, Font color: Text 1

Page 31: [11] Formatted **Marc Mallet** **11/8/16 11:22:00 PM**

Font:10 pt, Font color: Text 1

Page 31: [11] Formatted **Marc Mallet** **11/8/16 11:22:00 PM**

Font:10 pt, Font color: Text 1

Page 31: [11] Formatted **Marc Mallet** **11/8/16 11:22:00 PM**

Font:10 pt, Font color: Text 1

Page 31: [11] Formatted **Marc Mallet** **11/8/16 11:22:00 PM**

Font:10 pt, Font color: Text 1

Page 31: [11] Formatted **Marc Mallet** **11/8/16 11:22:00 PM**

Font:10 pt, Font color: Text 1

Page 31: [11] Formatted **Marc Mallet** **11/8/16 11:22:00 PM**

Font:10 pt, Font color: Text 1

Page 31: [11] Formatted **Marc Mallet** **11/8/16 11:22:00 PM**

Font:10 pt, Font color: Text 1

Page 31: [11] Formatted **Marc Mallet** **11/8/16 11:22:00 PM**

Font:10 pt, Font color: Text 1

Page 31: [11] Formatted **Marc Mallet** **11/8/16 11:22:00 PM**

Font:10 pt, Font color: Text 1

Page 31: [11] Formatted **Marc Mallet** **11/8/16 11:22:00 PM**

Font:10 pt, Font color: Text 1

Page 31: [11] Formatted **Marc Mallet** **11/8/16 11:22:00 PM**

Font:10 pt, Font color: Text 1

Page 31: [11] Formatted **Marc Mallet** **11/8/16 11:22:00 PM**

Font:10 pt, Font color: Text 1

Page 31: [11] Formatted **Marc Mallet** **11/8/16 11:22:00 PM**

Font:10 pt, Font color: Text 1

Page 31: [12] Formatted **Marc Mallet** **11/8/16 11:22:00 PM**

Font color: Text 1

Page 31: [12] Formatted **Marc Mallet** **11/8/16 11:22:00 PM**

Font color: Text 1

Page 31: [12] Formatted **Marc Mallet** **11/8/16 11:22:00 PM**

Font color: Text 1

Page 31: [12] Formatted **Marc Mallet** **11/8/16 11:22:00 PM**

Font color: Text 1

Page 31: [12] Formatted **Marc Mallet** **11/8/16 11:22:00 PM**

Font color: Text 1

Page 31: [13] Formatted **Marc Mallet** **11/8/16 11:22:00 PM**

Font color: Text 1

Page 31: [13] Formatted **Marc Mallet** **11/8/16 11:22:00 PM**

Font color: Text 1

Page 31: [13] Formatted **Marc Mallet** **11/8/16 11:22:00 PM**

Font color: Text 1

Page 31: [13] Formatted **Marc Mallet** **11/8/16 11:22:00 PM**

Font color: Text 1

Page 31: [13] Formatted **Marc Mallet** **11/8/16 11:22:00 PM**

Font color: Text 1

Page 31: [13] Formatted **Marc Mallet** **11/8/16 11:22:00 PM**

Font color: Text 1

Page 31: [14] Moved to page 23 (Move #1) **Marc Mallet** **5/2/17 1:32:00 AM**

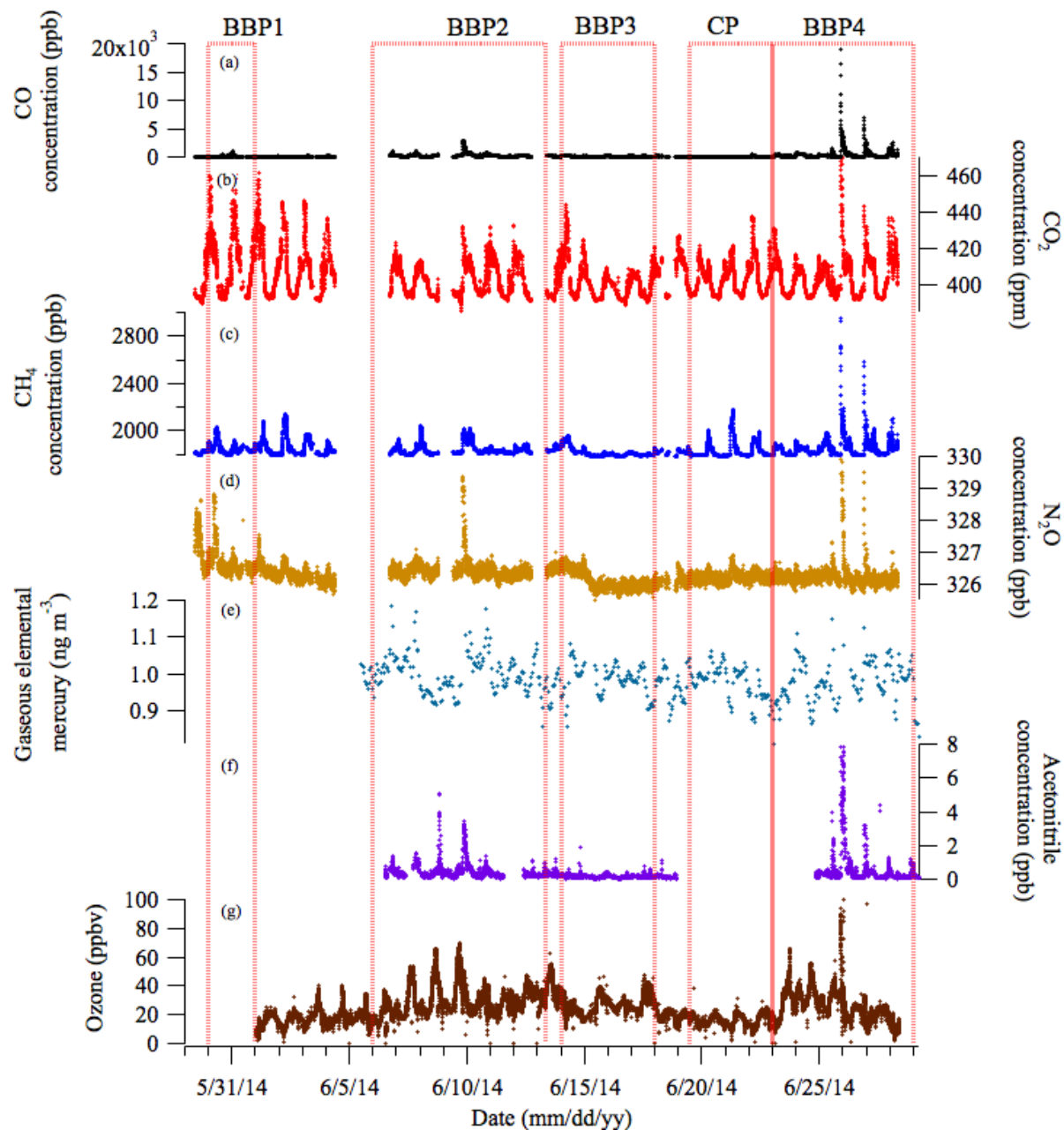


Figure 5 The time series of the major measured gaseous species during the SAFIRED campaign: (a) carbon monoxide, (b) carbon dioxide, (c) methane, (d) nitrogen dioxide, (e) gaseous elemental mercury, (f) acetonitrile and (g) ozone and $\Delta O_3/\Delta CO$. The biomass burning and coastal periods are indicated by the red dotted lines. All parts-per notation refer to mole fractions unless otherwise indicated.

Page 31: [15] Formatted	Marc Mallet	11/8/16 11:22:00 PM
--------------------------------	--------------------	----------------------------

Font color: Text 1

Page 31: [15] Formatted	Marc Mallet	11/8/16 11:22:00 PM
--------------------------------	--------------------	----------------------------

Font color: Text 1

Page 31: [15] Formatted	Marc Mallet	11/8/16 11:22:00 PM
--------------------------------	--------------------	----------------------------

Font color: Text 1

Page 31: [16] Moved to page 24 (Move #2)	Marc Mallet	5/2/17 1:32:00 AM
---	--------------------	--------------------------

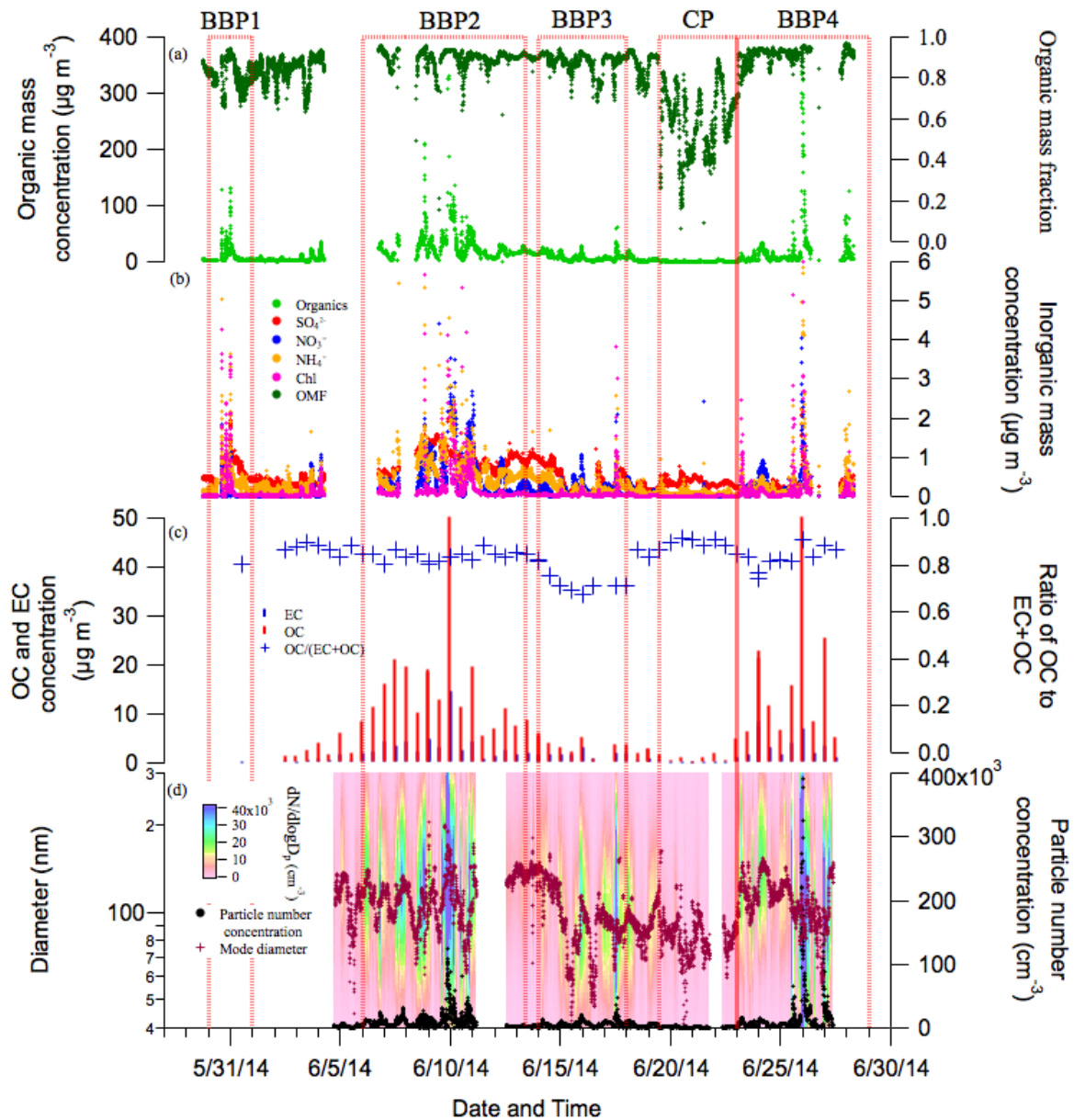


Figure 6 The times series of the major aerosol properties during the SAFIRED campaign: (a) the non-refractory PM₁ organic mass concentration (left) and organic mass fraction (right), b) the inorganic non-refractory PM₁ mass concentrations, (c) the 12-hour filter OC and EC PM₁ mass concentrations (left) and the ratio of OC to OC+EC (right), (d) the particle size distributions and particle size mode (left) and the total particle number concentration (right) and (e) the wind direction at ATARS.

Page 31: [17] Formatted

Marc Mallet

11/8/16 11:22:00 PM

Font color: Text 1

Page 31: [17] Formatted

Marc Mallet

11/8/16 11:22:00 PM

Font color: Text 1

Page 31: [17] Formatted **Marc Mallet** **11/8/16 11:22:00 PM**

Font color: Text 1

Page 31: [17] Formatted **Marc Mallet** **11/8/16 11:22:00 PM**

Font color: Text 1

Page 31: [17] Formatted **Marc Mallet** **11/8/16 11:22:00 PM**

Font color: Text 1

Page 31: [17] Formatted **Marc Mallet** **11/8/16 11:22:00 PM**

Font color: Text 1

Page 31: [17] Formatted **Marc Mallet** **11/8/16 11:22:00 PM**

Font color: Text 1

Page 31: [17] Formatted **Marc Mallet** **11/8/16 11:22:00 PM**

Font color: Text 1

Page 31: [18] Formatted **Marc Mallet** **11/8/16 11:22:00 PM**

Font color: Text 1

Page 31: [18] Formatted **Marc Mallet** **11/8/16 11:22:00 PM**

Font color: Text 1

Page 32: [19] Deleted **Marc Mallet** **5/14/17 10:42:00 PM**

BBP1, BBP2 and BBP4 correspond to the periods when fires were burning within 10 km of ATARS. Large enhancements of biomass burning related emissions were observed during these three periods. There were distinct enhancements of all measured gaseous and aerosol species during these periods. Differences between the maximum and background concentrations were very prominent for CO (note the logarithmic scale in Figure 5a), CH₄, N₂O, acetonitrile (an established marker for biomass burning) and organic, nitrate and chloride non-refractory sub-micron aerosol species. Similar enhancements of CH₄ were also observed outside of these BB periods, which

suggests another source of methane in this region. Only slight enhancements of GEM concentrations above background were observed during BBP2 and BBP4. Similar to much of the rest of the campaign sampling period, the non-refractory submicron aerosol was dominated by organics, with contributions typically varying between 70% and 95% of the mass. Relative to background concentrations, there were also large enhancements of nitrate and chloride species during these periods. While there were also enhancements of sulfate and ammonium species during these periods, similar enhancements were observed outside of these periods, again indicating a non-fire source of these species. The ratio of O_3 to CO concentrations above background (taken as 10 ppbv and 66 ppbv, respectively) gives an indication of the photochemical age of a smoke plume. $\Delta O_3/\Delta CO$ were lowest during BBP2 and BBP4 (and not measured during BBP1) relative to the rest of the campaign, indicating that the biomass burning signals during these periods had not undergone extensive photochemical aging and are therefore characteristic of fresh smoke.

Elevated signals during BBP1 were likely a result of a series of close fires within 5 km ENE of ATARS. The VIIRS and MODIS sensors on the SUMO NPP, Terra and Aqua satellites observes smaller fires at approximately 2 pm on the 30th of May. Winds were northeasterly during these two events. It is therefore likely that these signals were continuation or evolution of those fires. Burned vegetation was also visually observed the next morning at these locations. The large burst event later on the evening of the 31st of May is unlikely to be associated with these fires as the wind direction during this event was from the SSW and SSE. Large clusters of fires were observed at approximately 100 km and 150 km SE of the station by the Terra and Aqua satellites. The signals observed during this event could be a result of the plumes from this fire, although the possibility of a fire ignited after the satellite flyovers, or a combination of these cannot be eliminated.

Large signal enhancements on the 8th of June during BBP2 is likely a result of a cluster of fires approximately 100 km south east of the station. The MODIS sensors on the Terra and Aqua satellites observed the small cluster of fires along the back-trajectory at 11:14 am and 1:56 pm. The source of BB emissions for the large event on the 9th of June during this period is unclear. Several fires approximately 5 km from the station along the back-trajectory were detected by the MODIS sensor on Aqua and the VIIRS sensor on SUOMI NPP at approximately 2:30 pm on the 9th of June. There were also numerous fires detected between 100 km and 200 km southeast along this trajectory. The signals associated with this event could therefore be a result of the closer fires that started to blaze later in the evening, the distant fires or a combination of both.

Only one fire within 20km of ATARS was observed during BBP3 on the 17th of June. Numerous fires were observed further than 20km from the station and is possible that the signals during this period were more aged. While photochemical aging and coagulation typically lead to larger particles, particle size distributions were smaller during this period and the ratio of OC to OC+EC was 70%, 10% lower than the ratio during the rest of the campaign. Whether these observations were a result of burn conditions or aging processes

Page 32: [20] Deleted

Marc Mallet

5/14/17 10:42:00 PM

(i.e. evaporation of organic compounds from the aerosol phase) is unclear, although the highest $\Delta O_3/\Delta CO$ values during the campaign were observed during BBP3, which indicates photochemical aging was more extensive during this period.

One close fire was also observed during CP, however wind directions during this period were typically north-easterly and concentrations were therefore much lower. 5-day HYSPLIT

trajectories also show that air mass during the CP originated along the east coast of Australia before travelling towards the sampling station with very little terrestrial influence.

Close proximity fires

With numerous fires occurring across the region and the limitations of once-per-day satellite flyovers and stationary measurements, it can be difficult to identify the exact source of these elevated signals. For a portion of BBP4, however, fires were burning within several kilometers of ATARS and several plumes were easily observed from the station. The signals from these plumes are shown in Figure 8. The observed enhancements between 12:30 pm and 3:00 pm on the 25th June during BBP4 were a result of grass fires burning approximately 1 km south-east from the station. During this event, the wind direction (Figure 8k) was highly variable, changing between 140° and 80° True Bearing (TB) multiple times. As a result, the sampling changed from measuring the air mass with and without the plume from this fire, which led to sharp increases and decreases in biomass burning-related signals (Figure 8a through 8j). Visually, the fire area and extent of the plume was larger at 4:00pm than earlier, however the wind direction changed to north-easterly which directed the plume away from the station. From 4:00 pm until 10:00 pm, the wind direction was stable at approximately 50° TB. At 10:00 pm, the wind direction rapidly changed to directly south and the largest enhancements for the whole campaign were observed until approximately 2:00 am on the 26th of June. It is very likely that these signals were a result of a continuation and evolution of these fires as the night progressed. Portions of a ~0.25 km² grassland field within 500 m directly south of ATARS were observed to be burned upon arrival at the station on the morning of the 26th of June and we speculate that the burning of this field contributed to the large enhancements in measured biomass burning emissions. The emissions during this portion of BBP4

are likely to be the most representative of fresh biomass burning smoke during the SAFIRED campaign.

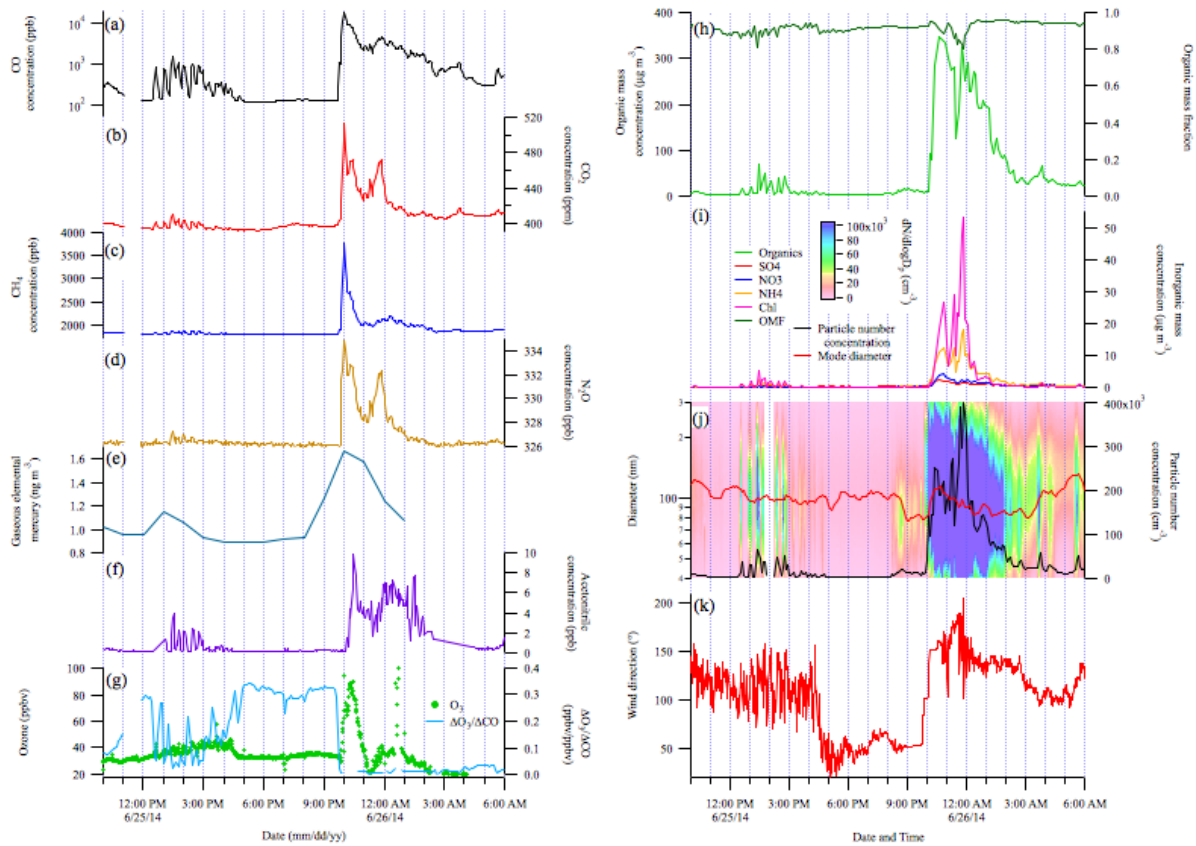


Figure 8 The major gas and aerosol concentrations measured during two biomass burning events within 1 km of ATARS during BBP4. (a) through (g) and (h) through (k) are as per Figures 5 and 6, respectively. All parts-per notation or mole fractions unless otherwise indicated.

Australian fires are responsible for 6% of global CO₂ biomass burning emissions, most of which is due to savannah fires (Shi et al., 2015). Carbon sequestering during regrowth periods is considered to balance carbon emissions in tropical Australia (Haverd et al., 2013). Greenhouse gases emitted from savannah fires that are not sequestered, such as methane (CH₄) and nitrous oxide (N₂O), have been shown to contribute 2-4% of the annual accountable greenhouse gas emissions from Australia (Meyer et al., 2012). Seasonal emission factors for the major greenhouse

gases are important for national greenhouse gas inventories and in understanding the impact of savannah fires. Furthermore, emission factors of CO₂ and CO can be used to infer mechanisms behind the emissions of other species, such as the connection between particulate matter and burning conditions.

The gaseous and aerosol data for the sample period were investigated to identify BB events and determine the emission factors of CO₂, CO, CH₄, N₂O, as well as Aitken and Accumulation mode aerosols and submicron particle species (organics, sulfates, nitrates, ammonium and chlorides) for several individual BB events. These emission factors were mostly found to be dependent on the combustion conditions (using the modified combustion efficiency as a proxy) of the fires. These results will be the first set of emission factors for aerosol particles from savannah fires in Australia. Furthermore, the variability in emission factors for different fires calls for a separation of single-value emission factors that are usually reported for savannah fires into grass and shrub components. A full discussion of these results are presented in Desservettaz et al. (2016, submitted).

Non-methane organic compounds (NMOCs)

Biomass burning is the second largest source of NMOCs globally with a recent global estimate of at least 400 Tg year⁻¹, second only to biogenic sources (Akagi et al., 2011). Biomass burning produces a complex mix of NMOCs, which may be saturated or unsaturated, aliphatic or aromatic, and contain substitutions of oxygen, sulfur, nitrogen, halogens and other atoms. NMOC emission rates are strongly tied to the efficiency of combustion, with smouldering fires emitting NMOC at higher rates than flaming fires (Andreae and Merlet, 2001). Biomass burning derived NMOCs fuel the production of tropospheric ozone in diluted, aged biomass burning plumes, with higher ozone

enhancements observed when biomass burning plumes interact with NO_x-rich urban plumes (Jaffe and Wigder, 2012; Wigder et al., 2013; Akagi et al., 2013). Oxidation of NMOCs results in lower volatility products that partition to the aerosol phase and contribute significantly to secondary organic aerosol (Hallquist et al., 2009). Biomass burning produces significant amounts of semi-volatile NMOC which can be difficult to quantify and identify with current measurement techniques. However recent studies have shown that including semi volatile NMOC chemistry in models improves the agreement between the modeled and observed organic aerosol (Alvarado et al., 2015; Konovalov et al., 2015) and ozone (Alvarado et al., 2015). High quality NMOC emission factors are crucial for models to assess the impact of biomass burning plumes on air quality and climate.

PAHs

Polycyclic aromatic hydrocarbons (PAHs) are a group of chemicals that are formed and emitted during combustion processes. Globally, major sources include residential/commercial biomass burning, open-field biomass burning and vehicular emissions (Shen et al., 2013). In Oceania in 2007, 31% of PAH emissions were estimated to be attributed to deforestation and wildfires (Shen et al., 2013). With control strategies targeting and reducing vehicular emission of PAHs over the last few decades, the relative contribution of other emission sources, such as savannah fires, has increased (Friedman et al., 2013; Kallenborn et al., 2012; Wang et al., 2016). Although most of these emissions are in the gas-phase (Jenkins et al., 1996; Atkins et al., 2010), the particle-phase PAHs, such as benzo[a]pyrene (BaP), may have high genotoxicity (IARC., 2015). However, field-based studies on emissions of PAHs from open-field biomass burning, including savannah fires remain limited in Australia (Freeman and Cattell, 1990).

Emission factors of PAHs from biomass burning related to savannah fires in northern Australia will be estimated from the data collected during this campaign. This estimation will be based on the (background subtracted) concentrations of PAHs and CO₂ (and CO) during the events where biomass burning contributes most to these concentrations measured at the sampling site. The concentrations of 13 major PAHs (gaseous plus particle-associated phase) varied from ~ 1 to over 15 ng m⁻³ within different BB events. In the gas phase, 3- and 4-ring compounds typically contributed ~ 90% to the sum concentrations whereas the particle-associated PAHs were dominated by 5- and 6-ring compounds (> 80%). Measured PAH concentrations were significantly higher (paired *t*-test, $P < <0.05$) during BB events E, F and G. For these events, concentrations of BaP exceeded the monitoring investigation level for atmospheric BaP in Australia (National-Environment-Protection-Council-Service-Corporation, 2011), i.e. 0.30 ng m⁻³, by 66% (BB event E) and 200% (BB events F and G). A full discussion of these results can be found in (Wang et al., 2016, under review).

Mercury

The atmosphere is the dominant transport pathway for mercury globally, with emissions to the atmosphere from both natural and anthropogenic origins (Driscoll et al., 2013). Whilst our understanding of the natural cycling of mercury has improved markedly over the past decades (Pirrone et al., 2010), large uncertainties still exist; specifically, global emission estimates to the atmosphere from biomass burning currently range between 300 and 600 Mg year⁻¹ (Driscoll et al., 2013). In the atmosphere, mercury exists as one of three operationally-defined species: gaseous elemental mercury (GEM), gaseous oxidised mercury (GOM) and particulate-bound mercury (PBM), each with differing abundances, solubility and depositional characteristics and with in-air conversion between all three species possible (Lin and Pehkonen, 1999). Mercury can be

scavenged from the atmosphere through both wet and dry depositional processes, and the monsoonal climate of northern Australia results in varying significance of each of these processes through the year (Packham et al., 2009). Upon deposition, mercury may be stored in plant tissue via stomatal or cuticular uptake (Rea et al., 2002) or sequestered within soils (Gustin et al., 2008). Release from both of these pools is achieved from burning events that may volatilise or thermally desorb mercury from biomass and soil, respectively (Melendez-Perez et al., 2014). Subsequently this mercury pool is redistributed through the atmospheric pathway to ecosystems that may methylate mercury, thereby enhancing its bioavailability to the local food chain.

SAFIRED represents the first measurements of atmospheric mercury undertaken in the tropical region of the Australian continent. The mean observed GEM concentration over the study period was $0.99 \pm 0.09 \text{ ng m}^{-3}$, similar to the average over that month (0.96 ng m^{-3}) for 5 other Southern Hemisphere sites and slightly lower than the average (1.15 ng m^{-3}) for 5 tropical sites (Sprovieri et al., 2016). Mean GOM and PBM concentrations were $11 \pm 5 \text{ pg m}^{-3}$ and $6 \pm 3 \text{ pg m}^{-3}$ respectively, representing 0.6 – 3.4% of total observed atmospheric mercury.

Atmospheric mercury measurements were available only during the final four identified burn events. During these events, spikes in GEM concentrations were observed, though there were no significant increases in GOM or PBM. Emission ratios calculated during the campaign were two orders of magnitude higher than those reported by Andreae and Merlet (2001), though those were from scrub, rather than grass, BB events (Desservettaz et al., 2016). Future outcomes from the SAFIRED campaign will focus on the use of micrometeorological techniques and the passive tracer radon to quantify delivery of atmospheric mercury to tropical savannah ecosystems. ATARS

also now serves as an additional site measuring continuous GEM as part of the Global Mercury Observation System (GMOS), one of only two tropical observing sites in the Eastern Hemisphere and the third such site located in Australia.

Aging of aerosols

Page 37: [24] Deleted

Marc Mallet

5/14/17 10:54:00 PM

Atmospheric chemistry and radiative forcing will depend on how gaseous and aerosol emissions from fires age as they move and interact with each other and existing species in the atmosphere. Biomass burning aerosols can be involved in condensation and coagulation (Radhi et al., 2012), undergo water uptake (Mochida and Kawamura, 2004) form cloud droplets (Novakov and Corrigan, 1996), and be exposed to photochemical aging processes, including those involving the gaseous components of fire emissions (Keywood et al., 2011;Keywood et al., 2015). With a reported lifetime of 3.8 ± 0.8 days (Edwards et al., 2006), biomass burning aerosols are able to travel intercontinental distances (Rosen et al., 2000) and are therefore present in the atmosphere long enough for substantial changes due to aging. Furthermore, tropical convection is likely to affect the aging of BB emissions in the region around ATARS, due to the immediate proximity to the warm waters in the Timor Sea (Allen et al., 2008). This introduces further uncertainty to the effect of BB emissions on radiation flux.

Primary organic aerosol directly emitted from biomass burning can interact with NMOCs to change composition and mass, resulting in secondary organic aerosol (Hallquist et al., 2009). Photochemical oxidation of NMOCs occurs during the daytime by either hydroxyl radicals or ozone. Ozone is also typically produced in the aging processes of tropical biomass burning plumes when NMOCs can oxidise to produce peroxy radicals that react with NO. Photochemical reactions

also may lead to an overall increase in total aerosol mass through the condensation of NMOCs onto existing particles (Reid et al., 1998; Yokelson et al., 2009; Akagi et al., 2012; DeCarlo et al., 2008). Some studies have shown the opposite, i.e., photo-oxidation can also lead to the evaporation of some primary organic constituents, resulting in an overall mass reduction (Hennigan et al., 2011; Akagi et al., 2012). With thousands of organic compounds in the atmosphere, each with different volatilities and potential reaction mechanisms, our understanding of secondary organic aerosol production is limited (Goldstein and Galbally, 2007; Keywood et al., 2011). Furthermore, secondary organic aerosol can also form through aqueous phase reactions where water-soluble organics dissolve into water on existing particles (Lim et al., 2010).

Further analysis into the aerosol chemical composition will elucidate the aging of early dry season biomass burning emissions. Fractional analysis (e.g., f_{44} and f_{60} , the fraction of m/z 44 and m/z 60 to all organic masses, indicated oxygenation and BB sources, respectively) and factor analysis using positive matrix factorisation (PMF) of cToF-AMS data has been investigated over the entire sampling period. Outside of the periods of significant influence from BB events, three PMF-resolved organic aerosol factors were identified. A BB organic aerosol factor was found to comprise 24% of the submicron non-refractory organic mass, with an oxygenated organic aerosol factor and a biogenic isoprene-related secondary organic aerosol factor comprising 47% and 29%, respectively. These results indicate the significant influence of fresh and aged BB on aerosol composition in the early dry season. The emission of precursors from fires is likely responsible for some of the SOA formation. A full discussion of these results can be found in Milic et al. (2016). Future analysis will investigate the gas and particle-phase composition for individual BB events.

Water uptake of aerosols

The water uptake by aerosols is determined by their size and composition, as well as the atmospheric humidity (McFiggans et al., 2006). The hygroscopic properties of all of the different components of an aerosol particle contribute to its total hygroscopicity (Chen et al., 1973; Stokes and Robinson, 1966). The presence of different water-soluble and water-insoluble organics and inorganics will therefore strongly influence water uptake. Furthermore, chamber studies that have investigated emissions from biomass fuels, both separately and in combination, have shown that the hygroscopic response can vary significantly depending on fuel type (Carrico et al., 2010). Understanding the water uptake of atmospheric aerosols is further complicated when considering other aging processes as described previously. Nonetheless, it is important to characterise the water uptake, as this will, in turn, influence other atmospheric chemistry processes, radiation scattering and absorption as well as cloud processing.

Biomass burning aerosols can act as cloud condensation nuclei if they are large enough for water to easily condense onto their surface, or if the particles have a large affinity for water due to their composition (Novakov and Corrigan, 1996). Ultimately, this means that BB emissions can lead to a higher number of cloud droplets. This is important in reflecting solar radiation and cooling the earth's surface. Cloud albedo is more susceptible to changes when cloud condensation nuclei concentrations are relatively low (Twomey, 1991), such as in marine environments like the Timor Sea off the coast of northern Australia.

The water uptake of aerosols has been further investigated to identify the possible influence of early dry season BB in this region on cloud formation. The concentrations of cloud condensation

nuclei at a constant supersaturation of 0.5% were typically of the order of 2000 cm^{-3} and reached well over 10000 cm^{-3} during intense BB events. Variations in the ratio of aerosol particles activating cloud droplets showed a distinct diurnal trend, with an activation ratio of $40\% \pm 20\%$ during the night and $60\% \pm 20\%$ during the day. The particle size distribution and the hygroscopicity of the particles were found to significantly influence this activation ratio. A full discussion of these results can be found in Mallet et al. (2016, submitted). Future analysis will elucidate the contribution of different biomass burning aerosol components on the hygroscopicity.

Trace metal deposition

The deposition and dissolution of aerosols containing trace metals into the ocean may provide important micronutrients required for marine primary production. Conversely, the deposition of soluble iron can trigger toxic algal blooms, such as *Trichodesmium*, in nutrient-poor tropical and subtropical waters (LaRoche and Breitbarth, 2005). *Trichodesmium* blooms require large quantities of soluble iron, of which aerosols are a source (Boyd and Ellwood, 2010; Rubin et al., 2011). To date, most studies have assumed that mineral dust aerosols represent the primary source of soluble iron in the atmosphere (Baker and Croot, 2010); however fire emissions and oil combustion are other likely sources (Ito, 2011; Schroth et al., 2009; Sedwick et al., 2007). A few studies have shown that iron contained in biomass burning emissions is significantly more soluble than mineral dust (Guieu et al., 2005; Luo et al., 2008; Schroth et al., 2009) but, to date, no data exists for Australian fires.

The aim of the trace metal aerosol component of SAFIRED is to quantify, for the first time, the fractional solubility of aerosol iron, and other trace metals, derived from Australian dry season BB. The fractional iron solubility is an important variable determining iron availability for

biological uptake. On a global scale, the large variability in the observed fractional iron solubility results, in part, from a mixture of different aerosol sources. Estimates of fractional iron solubility from fire combustion (1 - 60 %) are thought to be greater than those originating from mineral dust (1 - 2%) (Chuang et al., 2005;Guieu et al., 2005;Sedwick et al., 2007), and may vary in relationship to biomass and fire characteristics as well as that of the underlying terrain (Paris et al., 2010;Ito, 2011). Iron associated with BB may provide information with respect to BB inputs of iron to the ocean (Giglio et al., 2013;e.g. Meyer et al., 2008). The ATARS provides an ideal location to further investigate BB derived fractional iron solubility at the source. The results from this study can be found in Winton et al. (2016) and show that soluble iron concentrations from BB sources are significantly higher than those observed in Southern Ocean baseline air masses from the Cape Grim Baseline Air Pollution Station, Tasmania, Australia (Winton et al., 2015). Aerosol iron at SAFIRED was a mixture of fresh BB, mineral dust, sea spray and industrial pollution sources. The fractional iron solubility (2 - 12%) was relatively high throughout the campaign and the variability was related to the mixing and enhancement of mineral dust iron solubility with BB species.